B cell deficiency induces cytotoxic memory $CD8^+$ T cells during influenza-associated bacterial pneumonia

Leigh M. Miller[1], Alexis M. Duray[1], Ellyse M. Cipolla[1], Flavia Rago[1], Brooke P. Dresden[1], Kristen L. Parenteau[1], Abhigya Gupta[2], John F. Alcorn[1,3]

[1]Department of Pediatrics, UPMC Children's Hospital of Pittsburgh, Pittsburgh, PA, USA

[2]Dietrich School of Arts and Sciences, University of Pittsburgh, PA, USA

[3]Department of Immunology, University of Pittsburgh, Pittsburgh, PA, USA

Corresponding Author:

John F. Alcorn

9127 Rangos

4401 Penn Ave.

Pittsburgh, PA 15044

412-692-7595

john.alcorn@chp.edu

Keywords: antibody, lung, immunity, MRSA, mice

Funding: Supported by NIH R01 HL107380 (JFA) and Children's Hospital of Pittsburgh Research Advisory Committee Fellowship (LMM).

Author Contributions: Conceptualization, L.M.M and J.F.A; methodology, L.M.M, E.M.C, A.M.D, F.R, B.P.D, K.L.P, and A.G; data analysis, L.M.M; writing-original draft, L.M.M; writing- review and editing, L.M.M and J.F.A; supervision, J.F.A.

Declaration of interest: The authors have declared that no conflict of interest exists.

ABSTRACT:

Influenza-associated bacterial super-infections in the lung lead to increased morbidity and mortality. Nearly all people have pre-existing memory to influenza virus, which can protect against subsequent infection in the lung. This study explored the role B cells play in protection against bacterial (*Staphylococcus aureus* or *Klebsiella pneumoniae*) super-infection with previous heterotypic influenza memory. B cell deficiency resulted in an increased inflammatory lung environment and lung tissue injury during super-infection. Loss of B cells increased populations of memory $CD8^+$ T cells in the lung and these $CD8^+$ T cells were transcriptionally and functionally distinct from WT mice. Use of antibody-deficient mouse models showed that this phenotype was specifically due to loss of antibody production from B cells. Passive immunization with influenza-antibody serum in B cell deficient mice rescued the $CD8^+$ T cell phenotype. $CD8^+$ T cell depletion and lethal super-infection challenge experiments showed that the cytotoxic memory $CD8^+$ T cells from B cell deficient mice protect against super-infection bacterial burden and mortality. These findings provide insight into the importance of B cells for regulating immune responses against infection.

INTRODUCTION

Seasonal influenza annually contributes to significant morbidity and mortality among elderly, young, and immunocompromised persons. Influenza virus infection results in an inflammatory environment in which the lung epithelium becomes damaged (1-2). This process causes dysregulation of innate and adaptive immunity, leading to increased susceptibility to secondary bacterial pneumonias (3-6). Secondary bacterial pneumonias, particularly those caused by methicillin resistant *Staphylococcus aureus* (MRSA), result in increased morbidity and mortality during both seasonal influenza seasons and during the pandemics of 1918 and 2009 (7). Lung tissue impairment and long-term complications can occur (8). Mouse models have shown that immunity to bacterial infection in the lung is impaired by preceding anti-viral responses (9-16). Immune dysregulation by viral infection causes increased bacterial burden in the lung during super-infection, leading to increased lung inflammation and tissue injury compared to single infection (17-18). It is critical to develop an understanding of how immune mechanisms become dysregulated during influenza-associated bacterial pneumonias.

Following clearance of influenza virus, innate and adaptive immune systems form memory. Influenza virus is coated with surface antigens hemagglutinin (HA) and neuraminidase (NA). Memory B cells primarily secrete neutralizing antibodies targeted against HA and NA (19-21). However, antigenic drift of HA and NA decreases the efficiency of the pre-existing antibody repertoire over time, rendering pre-formed antibodies ineffective against heterotypic influenza virus infection (19-21). Lack of cross-protective antibodies against influenza virus is a primary reason why seasonal influenza

vaccines need to be reformulated annually (19-21). Influenza viruses also contain conserved internal antigens, such as nucleoprotein (NP), that are less susceptible to mutating (21-22). Memory $CD4^+$ and $CD8^+$ T cells recognize these internal viral epitopes, making them highly effective at providing cross-protective responses against heterotypic influenza viruses (21-25). Following clearance of influenza virus, T cells form memory subsets, such as central memory, effector memory, and resident memory. Lung tissue resident memory T cells (TRMs) have been shown to provide optimal protection against influenza virus and are critical for providing heterosubtypic immunity. $CD8^+$ TRMs primarily act to detect re-infection at sites of pathogen entry and secrete cytokines, such as IFNγ, TNFα, and granzymes, to mediate anti-viral immunity (23-27). However, cytotoxic memory $CD8^+$ T cells may act as a "double edged sword"; $CD8^+$ T cell activation is essential for viral and bacterial clearance but may also contribute towards increased tissue damage (28-30).

A majority of studies relating to influenza-associated bacterial infections focus on acute disease in previously naïve mice, however, nearly all humans have pre-existing immunity to influenza virus and repeat infection with the same influenza virus strain is uncommon (31). Therefore, an influenza-associated bacterial pneumonia model that takes pre-existing heterotypic influenza memory into account may be more clinically relevant. Our group previously showed that prior challenge with heterosubtypic influenza virus in mice improves control of subsequent super-infection and reduces lung tissue injury (32). Because lung memory B and T cells are key arms of pre-existing immunity, we explored the functional role of B cells for heterotypic protection. Using spectral flow cytometry and transcriptomics, we studied the importance of B cells for

clearance of pathogen and prevention of tissue injury in the lung. B cells were manipulated using genetic and temporal antibody depletion and passive transfer of influenza antibody serum. These data demonstrate the functional role of B cells in heterotypic influenza virus strain immunity and how loss of B cell function impacts formation of lung memory $CD8^+$ T cells and exacerbates lung inflammation following heterotypic influenza virus strain super-infection.

RESULTS

MRSA challenge following heterotypic influenza memory increases tissue injury in the lung and alters the innate cell compartment

To investigate how B cells impact immune memory during super-infection, we primed WT or B cell deficient (μMT) mice with influenza A/HKx31 (H3N2, X-31) virus on day 0, followed by rechallenge with a heterotypic strain of influenza A/PR/8/34 (H1N1, PR8) virus at day 54. Six days following PR8 challenge, mice were inoculated with MRSA USA300 or PBS, and tissues were harvested 24 hours later (Figure 1A). We used mouse-adapted strains X-31 and PR8 as they have similar internal proteins while expressing dissimilar proteins on their surface. These influenza viruses have been used previously by others, and this pre-existing influenza memory super-infection model (Figure 1A) has been characterized by our group (32-34). Prior experiments examined how the addition of heterotypic influenza memory impacted control of super-infection (F/F/S) compared to acute infection (F/S). WT mice with F/F/S infection lost significantly less weight compared to WT mice with F/S infection, but heterotypic memory did not impact weight loss in μMT mice (Figure S1A)(32). Interestingly, both WT and μMT mice with F/F/S infection had lower lung MRSA burden and viral burden compared to their F/S controls (Figure S1B-C). Because bacterial and viral burden was not significantly different between WT and μMT mice during F/S or F/F/S infection, we investigated whether lung tissue injury was different. We measured lung tissue injury using two methods: sample blinded scoring by investigators or Qupath, which allowed us to measure immune cell infiltration and lung tissue inflammation using machine-learning based algorithms. Comparing lung tissue injury in F/S mice versus F/F/S mice showed

that there was no significant change in lung tissue injury between WT and µMT mice during F/S infection (Figure S1D). However, WT mice had improved control of parenchymal tissue injury during F/F/S infection, but this was not that case with µMT mice, which had significantly more parenchymal tissue injury compared to WT mice (Figure S1D).

To further assess the impact of MRSA challenge on the lung inflammatory environment during B cell deficiency, we compared lung tissue injury in WT and µMT mice during memory heterotypic influenza virus (F/F) or memory super-infection (F/F/S). Using Qupath, mice with F/F infection trended towards decreased lung inflammation and consolidation (dense areas with no space for air exchange) compared to F/F/S regardless of genotype, but this finding was not statistically significant (Figure S2A). We then assessed tissue integrity by measuring protein leak into airspaces and found significantly higher levels of protein in the bronchoalveolar lavage fluid (BALF) of WT and µMT mice that received F/F/S infection compared to mice with F/F infection (Figure S2B). Using Qupath, we overlayed a heatmap highlighting areas of inflammation and consolidation; this showed that WT and µMT mice had more lung inflammation during F/F/S infection compared with F/F infection (Figure 1B). B cell deficiency trended towards a moderate increase in cell density and inflammation in the lung during F/F infection compared to WT, but these data were not statistically significant. However, we found that during F/F/S infection, B cell deficiency significantly increased lung tissue injury and cell density in the lung compared to WT mice (Figure 1C).

Next, we explored how MRSA challenge altered the lung immune cell compartment with heterotypic memory influenza virus infection in WT and µMT mice.

Using conventional flow cytometry gating (Figure S3) and dimensionality reduction (tSNE-CUDA) and clustering (FlowSOM), we tracked changes of the innate and adaptive immune cell compartments in lungs (Figure 1D). We observed larger populations of T cells and macrophages (interstitial and exudate) in the lungs of µMT compared to WT mice (Figure 1D-E, Figure S2C). Additionally, we found greater numbers of both M1-like (iNOS^{+} MHCII^{high}) and M2-like (CD206^{+}) macrophages in the lungs of µMT compared to WT mice (Figure 1F, Figure S2D). We also found more NK cells in the lungs of µMT mice compared to WT (Figure S2E). We found that the largest change in the immune cell compartment of F/F versus F/F/S mice following MRSA challenge was an increase in the number of neutrophils (Figure 1D, Figure S2F). While the number of neutrophils did not change between WT and µMT lungs, the neutrophils of µMT lungs were proportionally more mature and expressed higher levels of iNOS, a key regulator of neutrophil function (Figure S2G-H). Additionally, we observed an increase in genes related to neutrophil function in WT mice during F/F/S challenge compared to F/F challenge with gene expression unchanged between µMT F/F and F/F/S infection (Figure S2I). We saw that the number of B cells in the lung tissue of WT mice significantly decreased following MRSA challenge (Figure 1D, Figure S2J). We additionally compared viral burden between WT and µMT F/F and F/F/S groups and observed no significant differences between infection groups (Figure S2K). Next, we compared changes in inflammatory cytokines/mediators in the lungs of both WT and µMT mice. For both WT and µMT mice, we observed increases in some pro-inflammatory cytokines (IL-1α, IL-1β, IL-6, IL-12p40) and other mediators that promote neutrophil chemotaxis to the lung (G-CSF, KC/CXCL1) following MRSA challenge

(Figure S2L). Unlike μMT mice, the lungs of WT mice had significantly higher expression of mediators that promote macrophage migration (MCP-1, MIP-1α, MIP-1β), which may reflect the higher number of macrophages already present in the lungs of μMT mice prior to MRSA challenge (Figure 1E, Figure S2C). Another interesting finding was that IL-10 was decreased in the lungs of both WT and μMT mice following MRSA challenge (Figure S2L). Together these data show that MRSA challenge altered the lung environment of both WT and μMT mice towards a state of higher inflammation, but μMT mice had larger populations of T cells and macrophages in the lung compared to WT during F/F and F/F/S infection.

Absence of B cells increases formation of cytotoxic effector $CD8^+$ T cells in the lung

It has been shown by others that heterotypic strain control of influenza virus is largely T cell-dependent (22-23). To further characterize the changes in the T cell compartment of WT and μMT mice during F/F and F/F/S infection, we examined marker expression changes of T cells in the lung. Using our T cell gating strategy (Figure S4), we found that $CD4^+$ and $CD8^+$ T cells were significantly increased in both number and proportion in the lungs of μMT compared to WT mice, during both F/F infection and F/F/S infection, with $CD4^+$ and $CD8^+$ T cells decreased in the lung due to MRSA challenge (Figure 2A-C, Figure S5A-C). Additionally, μMT lungs had significantly higher numbers of effector memory and TRM $CD8^+$ T cells compared to WT lungs during both F/F infection and F/F/S infection (Figure 2D, Figure S5D). Next, we examined the functional phenotype of these effector $CD8^+$ T cells by examining expression of transcription factors and pro-inflammatory cytokines. We observed that the majority of

lung $CD8^+$ T cells of μMT mice expressed granzyme B, a marker of cytotoxicity, whereas WT lungs had a lower proportion and absolute number of granzyme B^+ $CD8^+$ T cells (Figure 2E). Next, we looked at expression of a key anti-viral cytokines, IFNγ and TNFα, and found that the lung $CD8^+$ T cells of μMT mice had significantly lower expression of these cytokines compared to WT (Figure 2F-G). However, we did not find lower expression of Tbet in the lung $CD8^+$ T cells of μMT, indicating that these $CD8^+$ T cells have impaired cytokine production (IFNγ, TNFα), but not impaired differentiation into an anti-viral effector phenotype (Figure 2F-H). Interestingly, MRSA challenge in WT mice (F/F/S) significantly decreased the proportion of lung $CD8^+$ T cells expressing IFNγ and TNFα compared to F/F infection, which further highlights the immune dysfunction caused by secondary MRSA infection. These data show that B cell deficiency increases the population of effector and resident memory $CD8^+$ T cells in the lung and alters their functional phenotype.

We next explored whether this phenotype was unique to heterotypic infection by comparing heterotypic influenza super-infection with homotypic influenza (PR8-PR8) super-infection. WT and μMT mice lost more weight during heterotypic infection compared to homotypic infection (Figure S6A). While bacterial burden was unchanged between groups, viral burden was increased in μMT mice with heterotypic infection compared to homotypic infection (Figure S6B-C). For both WT and μMT mice, no significant differences were observed in the innate immune cells (neutrophils, macrophages) (Figure S6D-E). Heterotypic influenza infection resulted in an increase in effector memory and TRM $CD8^+$ T cells in the lungs of both WT and μMT mice compared to homotypic infection (Figure S6F-G). Interestingly, there was an increase in

the proportion of influenza-specific $CD8^+$ T cells in WT mice with heterotypic infection compared to homotypic infection, but not in the lungs of μMT mice (Figure S6H). For both heterotypic and homotypic influenza infections, $CD8^+$ T cells of μMT mice had higher co-expression of PD-1, LAG-3, and TIM-3 compared to WT; however, this co-expression was greater in heterotypic infection compared to homotypic infection for both WT and μMT mice (Figure S6I). Additionally, granzyme B concentration in the BALF was increased with heterotypic infection compared to homotypic infection for WT and μMT mice (Figure S6J). Lung tissue injury was increased in heterotypic infection compared to homotypic infection in WT mice, but this finding was not statistically significant for μMT mice (Figure S6K). Overall, these data show that the unique $CD8^+$ T cell phenotype of B cell deficient mice is still observed in homotypic influenza infection, but the phenotype is more pronounced in heterotypic influenza infection.

Lung $CD8^+$ T cells from B cell deficient mice have an altered transcriptional profile

To further assess the differences in lung $CD8^+$ T cells between WT and B cell deficient (μMT) mice, we sorted the $CD8^+$ T cells from the lungs of F/F and F/F/S infected WT and μMT mice and performed bulk-RNA-sequencing. We examined the sample clustering using PCA analysis and found that the lung $CD8^+$ T cells from the WT mice (F/F and F/F/S) had more similarity with each other than with either of the μMT groups (F/F and F/F/S) (Figure S7A). We examined how MRSA challenge impacts the transcriptional profile of $CD8^+$ T cells in the lung. The $CD8^+$ T cells of WT mice had more differentially expressed genes (2084) between F/F and F/F/S groups compared to μMT lung $CD8^+$ T cells, which had fewer differentially expressed genes (71) (Figure 3A). The

shared genes (43) between the two were related to cell movement and migration (Figure S7B). Interestingly, Gene Ontology (GO) pathways and differentially expressed genes associated with immune-response signaling, immune cell activation, and control of bacterial infection were downregulated in F/F/S compared to the F/F group in WT mice, suggesting that secondary bacterial challenge in the lung significantly dysregulated immune responses, in particular the Type 17 pathway (Figure S7C-D). We looked at the transcriptional differences of lung $CD8^+$ T cells between WT and µMT mice during F/F and F/F/S infection (Figure 3B, Figure S7E-F). The pathways enriched in F/F/S µMT mice were associated with adaptive immune response, cell regulation, and response to bacterial stimulus (Figure 3B). We examined transcriptional genes associated with T cell effector function, as well as genes associated with regulation of T cell activation (35-38). We found significant upregulation of several of these markers in µMT mice compared to WT mice during F/F/S infection (Figure 3C). Flow cytometry analysis of lung $CD8^+$ T cells co-expressing PD-1, TIM-3, and LAG-3 showed that these markers were significantly upregulated in µMT compared to WT mice and were also increased in proportion upon MRSA challenge (Figure 3D). Intravascular staining further showed that the population of $CD8^+$ T cells co-expressing PD-1, TIM-3, and LAG-3 in µMT mice was concentrated in the lung tissue versus the peripheral blood (Figure S7G). Gene set enrichment analysis (GSEA) for biological pathways showed that $CD8^+$ T cells in µMT lungs were enriched for apoptosis signaling and flow cytometry analysis confirmed that B cell deficiency during F/F/S infection increased the frequency of apoptotic $CD8^+$ T cells in the lung (Figure 3E). Overall, these data show that loss of B

cells has a profound impact on the transcriptional profile of lung $CD8^+$ T cells, causing upregulation of several genes associated with T cell regulation and effector function.

Loss of influenza virus-specific antibody increases formation of cytotoxic effector $CD8^+$ T cells in the lung during subsequent super-infection

We sought to determine which B cell function was causing the distinct $CD8^+$ T cell phenotype observed in µMT mice. To examine the role of memory B cell-antibody secretion during subsequent super-infection, we used four different strains of mice: WT C57BL/6 mice, B cell deficient mice (µMT), MD4 mice, and IgMi mice. MD4 mice, which have a transgenic B cell receptor specific to hen egg lysozyme (HEL), produce ten times fewer virus-specific precursor splenic B cells compared to WT mice (39). During F/F/S infection, MD4 mice produced influenza virus X31-specific antibody, but at significantly lower levels compared to WT mice (Figure 4A). IgMi mice failed to produce any soluble antibody, similar to µMT mice, as all constant regions in the IgH chain are deleted, preventing class-switching from IgM (40). We showed that MD4 mice represent an intermediate influenza virus-specific antibody deficient mouse strain in our study, while the IgMi mice are a complete influenza virus-specific antibody knock-out (Figure 4A). WT mice lost significantly less weight compared to our B cell deficient strains (µMT, MD4, and IgMi) with µMT and IgMi mice having lost more weight than the MD4 mice, suggesting that weight loss during F/F/S infection is dependent on the presence of pre-existing influenza virus-specific antibody (Figure 4B). While µMT mice had more viral burden in the lung compared to WT mice, a majority of mice in all four groups (µMT, MD4, and IgMi) had non-detectable levels of PR8 gene expression (Figure 4C).

Interestingly, all four groups had similar amounts of bacterial burden, suggesting that bacterial clearance is not antibody-dependent (Figure 4D).

We examined T cell populations during F/F/S infection and saw a significant increase of lung $CD8^+$ T cells in all three B cell deficient mouse strains (μMT, MD4, and IgMi) (Figure 4E, Figure S8A). A majority of these $CD8^+$ T cells were effector memory phenotype (Figure 4F). Additionally, we observed a significant increase in lung $CD4^+$ T cells (Figure S8B-C). Loss B cells or influenza virus-specific antibody increased the absolute number of influenza virus -specific and tissue resident memory (TRM) $CD8^+$ T cells in the lung (Figure 4G, Figure S8D). Within the $CD8^+$ T cell population, we examined surface markers commonly related to T cell regulation (PD-1, LAG-3, TIM-3) and found significantly increased expression in all three B cell deficient mouse strains (μMT, MD4, and IgMi) with lower expression found in MD4 mice (Figure 4H). Next, we analyzed which cytokines the $CD8^+$ T cells were producing in response to F/F/S infection and found significantly lower expression of IFNγ in μMT and IgMi mice (Figure 4I). However, the $CD8^+$ T cells of B cell deficient mice (μMT, MD4, and IgMi) had high expression of the effector molecule granzyme B as well as elevated concentrations of granzyme B in the BALF, suggesting that loss of B cell antibody induces more cytotoxic lung $CD8^+$ T cells (Figure 4J-K). Finally, we examined the repertoire of inflammatory cytokines expressed in WT and B cell deficient (μMT, MD4, and IgMi) lungs and BALF and found that certain pro-inflammatory cytokines, such as TNFα, were decreased in B cell deficient mice (μMT, MD4, and IgMi) (Figure 4L, Figure S8E). However, cytokines that promote activation of the innate immune compartment (IL-6, MCP-1/CCL2, MIP-1β/CCL4, G-CSF) were increased in B cell deficient mice (μMT, MD4, and IgMi) (Figure

S8E-F). These data suggest that while influenza virus-specific antibody is not necessary for control of bacterial super-infection burden, specific loss of influenza virus-specific antibody results in formation of cytotoxic effector memory $CD8^+$ T cells in the lung.

Loss of influenza virus-specific antibody increases lung tissue injury during memory super-infection

A heatmap overlay highlighting areas of inflammation and consolidation showed that lungs of WT mice had inflammation during F/F/S infection, but µMT and IgMi lungs comparatively had more intense inflammation visually with MD4 lungs resembling WT lungs (Figure 5A). Sample blinded pathology scoring of WT and B cell deficient (µMT, MD4, and IgMi) mice highlighted the increased immune cell infiltration and inflammation surrounding the blood vessels and airways of µMT and IgMi mice compared to WT and MD4 mice during F/F/S infection (Figure 5B-C). Qupath analysis showed significantly increased immune cell density in the lungs of µMT and IgMi compared to WT mice during F/F/S infection (Figure 5D). Additionally, the frequency of inflammation and consolidation of the lungs was significantly increased in all three B cell deficient strains (µMT, MD4, and IgMi) compared to WT during F/F/S infection (Figure 5E). Using BALF, we observed significantly increased lung leak in B cell deficient mice (µMT, MD4, and IgMi) compared to WT during F/F/S infection (Figure 5F). These data indicate that loss of influenza virus-specific antibody production from B cells leads to increased lung tissue injury during F/F/S infection.

Depletion of B cells increases formation of cytotoxic, effector memory CD8$^+$ T cells in the lung

Next, we wanted to examine whether the cytotoxic, effector memory CD8$^+$ T cells in the lung resulted from loss of influenza virus-specific antibody during primary influenza (X-31) virus infection or from loss of influenza virus-specific antibody during the entirety of our F/F/S model. To accomplish this, we used MD4 mice, which already have an attenuated influenza virus-specific B cell and antibody response. We depleted B cells in the lungs prior to primary influenza virus (X-31) infection and allowed B cells to repopulate the lung before secondary influenza virus infection (Figure 6A). Using flow cytometry, we confirmed depletion of B cells in the lung on the day of primary influenza virus challenge using a B cell depleting antibody or isotype control (IgG2b). We observed that the B cells began to repopulate the lung as soon as 30 days following primary influenza virus infection (Figure 6B). To confirm loss of antibody during primary influenza virus infection, we assessed the serum titer of X-31-specific antibody on the day of harvest and saw a significant decrease in B cell depleted mice compared to the isotype controls (Figure 6C). We observed that mice with B cell depletion lost more weight during F/F/S infection compared to the isotype group, further demonstrating that weight loss during influenza virus infection was antibody-dependent (Figure 6D). Although not statistically significant, we observed moderately increased lung tissue injury in the B cell depleted group during F/F/S infection (Figure 6E-F). Consistent with previous observations, B cell loss during primary infection did not impact MRSA burden in the lung during F/F/S infection (Figure 6G). We looked at lung CD8$^+$ T cells and found that the B cell depleted group had a significantly larger proportion of CD8$^+$ T cells in the

lung compared to the isotype group (Figure 6H). Additionally, there was a significant increase of $CD8^+$ lung TRMs and $PD\text{-}1^+$ CD8 T cells in the B cell depleted group compared to the isotype group (Figure 6I-J). Depletion of B cells also increased the concentration of granzyme B in the BALF compared to the isotype controls (Figure 6K). Overall, these data show that loss of influenza virus-antibody generated in response to primary challenge with influenza virus increases formation of TRM $CD8^+$ T cells in the lung.

We next depleted B cells prior to secondary influenza challenge to explore whether loss of B cells in the lung impacts control of super-infection and $CD8^+$ T cell phenotype (Figure S9A). B cell depletion at this time point did not impact weight loss despite efficient B cell depletion in the lung, likely due to sustained high titers of influenza specific antibody (Figure S9B-D). Interestingly, MRSA burden decreased in the lungs of B cell depleted mice, but macrophage and neutrophil populations were unchanged between groups (Figure S9E-G). Additionally, total lung $CD8^+$ T cells, memory $CD8^+$ T cells (TRMs), and $PD\text{-}1^+$ $CD8^+$ T cells were not impacted by B cell depletion prior to secondary influenza challenge (Figure S9H-J). We also did not observe any differences in lung injury between groups (Figure S9K). Overall, these data show that the presence of B cells in the lung at the heterotypic strain challenge time point is not crucial for control of super-infection.

Passive antibody serum immunization improves control of super-infection in B cell deficient mice

Next, we passively immunized WT and μMT mice several hours following secondary influenza infection (PR8) with either memory serum collected and pooled from memory super-infected WT mice, naïve serum collected and pooled from WT mice, or PBS vehicle. We observed that μMT mice that received memory serum had significantly less weight loss compared to the naïve serum and PBS control groups, further showing that weight loss is antibody-dependent (Figure 7A). Next, we looked at viral and bacterial burden and did not observe statistically significant differences between the groups (Figure S10A-B). Interestingly, while we observed a decrease in total and influenza-specific lung $CD8^+$ T cells in the lungs of μMT mice that received memory serum compared to controls, the proportion of $CD8^+$ T cells that were effector memory did not change between groups (Figure 7B-C, Figure S10C). Additionally, the proportion of $CD8^+$ T cells expressing PD-1 decreased in μMT mice that received memory serum compared to controls (Figure 7D). We then examined the innate immune compartment and found that the number of macrophages decreased in the lungs of μMT mice that received memory serum with the frequency of activated ($CD40^+$) macrophages also decreased compared to controls (Figure 7E, Figure S10D). There was a trending decrease of NK cells and neutrophils in the lungs of μMT mice that received memory serum compared to controls, but no significant differences in number of dendritic cells (Figure S10E-G). We determined if passive immunization rescued lung tissue injury, and we observed decreased lung tissue injury in μMT mice that received memory serum compared to vehicle and naïve serum controls (Figure 7F, Figure S10H-I). Additionally, we observed a decrease in the amount of secreted granzyme B in the BALF of μMT mice that received memory serum compared to controls (Figure 7G).

These data demonstrate that passive immunization with influenza specific antibody serum rescues many of the phenotypes associated with B cell deficiency.

B cell antibody deficiency has a similar impact on CD8$^+$ T cells in influenza virus, Klebsiella pneumoniae super-infection

After we observed a unique CD8$^+$ T cell phenotype and worsened lung injury in secondary bacterial infection with MRSA in antibody-deficient mice, we examined whether our findings would be consistent with a different bacterial pathogen. To do this, we used *Klebsiella pneumoniae* (Kp), a Gram-negative bacterium that is highly virulent in mice (Figure S11A). We observed increased weight loss in IgMi mice compared to WT mice (Figure S11B). Unlike with F/F/S infection, bacterial burden increased in IgMi mice compared to WT (Figure S11C). We then measured tissue integrity by BALF protein concentration and observed a significantly higher concentration in IgMi mice compared to WT (Figure S11D). Looking at the innate immune cell compartment, we observed increased macrophages in the lungs of IgMi compared to WT mice, but not neutrophils (Figure S11E-F). Similar to F/F/S infection, the lungs of IgMi mice with F/F/Kp infection had higher numbers of total CD8$^+$ T cells, CD8$^+$ TRMs, influenza-specific CD8$^+$ T cells, and CD8$^+$ T cells co-expressing PD-1, LAG-3, and TIM-3 (Figure S11G-J). We additionally observed significantly more granzyme B secretion in the BALF of IgMi compared to WT mice (Figure S11K). Overall, these data show that the phenotype we see in F/F/S infection was observed in super-infections with a different pathogenic bacteria; however, IgMi mice appear to have impaired control of *Klebsiella pnuemoniae* burden.

Effector cytotoxic CD8$^+$ T cells induced by B cell deficiency are protective against lethal secondary bacterial pneumonia

To assess whether memory effector CD8$^+$ T cells in the lung were protective or detrimental during secondary bacterial infection, we depleted CD8β$^+$ T cells (IV and IT) in WT and μMT mice prior to challenge with influenza (PR8) virus (Figure 8A). Lung CD8β$^+$ T cell depletion was confirmed on the day of tissue harvest using flow cytometry (Figure 8B). We observed that depletion of CD8β$^+$ T cells in μMT mice resulted in significantly higher MRSA burden in the lung compared to controls (Figure 8C). Additionally, μMT lungs depleted of CD8β$^+$ T cells had significantly higher viral burden (PR8) compared to WT and isotype groups (Figure 8D). This suggests that the cytotoxic memory CD8$^+$ T cells of μMT are protective against influenza virus and MRSA challenge; however, depletion of CD8$^+$ T cells in WT mice did not significantly impact influenza virus or MRSA burden, likely due to the presence of antibody. Because we observed previously that B cell deficient mice (μMT, MD4, and IgMi) formed lung CD8$^+$ T cells with increased granzyme B expression, we analyzed the concentration of granzyme B in the BALF. We observed that μMT mice with CD8β T cell depletion had moderately decreased granzyme B concentration in the BALF, although this did not reach statistical significance. There was no difference in granzyme B concentration in the BALF of WT groups (CD8$^+$ T cell depleted vs. isotype), demonstrating that effector cytotoxic lung CD8$^+$ T cell formation is a unique feature of B cell deficiency (Figure 8E). We did not observe any differences in lung tissue injury between CD8β$^+$ T cell depleted

443 and isotype groups (Figure S12A). However, we saw a significant increase of lung $CD4^+$
444 T cell number, IL-6, and BALF neutrophil frequency in μMT mice that were depleted of
445 $CD8\beta^+$ T cells, suggesting that other immune cells were recruited to the lungs to control
446 super-infection (Figure S12B-D).

447 Since we saw that $CD8^+$ T cells are important for MRSA clearance in the lungs of
448 μMT mice, we wanted to assess their ability to control secondary bacterial pneumonia
449 by challenging WT and μMT mice with a lethal dose ($2x10^8$ CFU) of MRSA in our model.
450 We observed that μMT mice lost more weight than WT mice (Days 54-60), which was
451 dependent on influenza virus (PR8) infection. WT mice lost a significant amount of
452 weight in the 48 hours following MRSA challenge (Days 60-62), suggesting that weight
453 loss in WT mice is primarily dependent on secondary bacterial infection (Figure 8F).
454 Overall, WT and μMT groups had similar mortality rates following lethal super-infection,
455 but the time points at which mortality occurred significantly differed. Mortality in the WT
456 group occurred 24-48 hours post- MRSA challenge, suggesting that WT mice were not
457 able to effectively clear MRSA infection (Figure 8G). The μMT group experienced less
458 mortality 24-48 post-MRSA challenge (20%) compared to WT mice (65%) (Figure 8G).
459 These data suggest that the μMT mice were able to control the MRSA infection more
460 effectively than the WT group despite already experiencing significant weight loss due to
461 influenza virus infection. 48 hours post-MRSA challenge, both μMT and WT groups
462 began to recover from the weight loss; however, some individual μMT mice continued to
463 lose weight and were euthanized at days 63, 64, and 65 (Figure 8F-G). The continued
464 mortality 72-96 hours post-MRSA challenge in the μMT group was likely due to
465 antibody-dependent weight loss and from the inflammatory lung environment. To

466 determine whether the increased early mortality in WT mice was due to increased
467 MRSA burden, we examined bacterial burden 14 hours post lethal MRSA challenge and
468 observed increased burden in WT compared to μMT mice (Figure 8H). When
469 heterotypic memory experienced WT and μMT mice were challenged with lethal MRSA
470 without secondary PR8 influenza virus challenge (Figure S12E), both groups had ~ 50%
471 mortality within 48 hours of challenge (Figure S12F-G). Overall, these data suggest that
472 loss of B cells induces formation of lung cytotoxic effector $CD8^+$ T cells, which promote
473 acute control of MRSA challenge during F/F/S infection.
474

DISCUSSION

Pulmonary infections caused by viruses, such as influenza virus and SARS-COV-2, remain a persistent public health burden globally. Immune dysregulation following viral infection increases susceptibility to developing secondary bacterial pneumonias, resulting in increased morbidity and mortality rates (5, 7-8). Studies on naïve mice have shown that altered immune responses during preceding viral infection hinders anti-bacterial mechanisms during secondary bacterial pneumonia (9-16). Our group has previously shown that mice with heterotypic influenza memory have better controlled immunopathology and improved bacterial clearance in the lung (32). The data presented in this study expand on this knowledge and show that previous influenza virus infection alters immune responses against secondary bacterial infection. $CD8^+$ T cells are crucial for controlling heterotypic influenza infection by recognizing and killing virally infected cells, but less is known about their responses to extracellular bacterial infections. While primarily an extracellular infection, MRSA can invade phagocytic cells. $CD8^+$ T cells can lyse and kill these infected cells via perforin and granzyme B (41-42). Our analysis of sorted lung $CD8^+$ T cells in WT mice showed transcriptomic differences between F/F and F/F/S groups. Th17 derived-cytokines and antimicrobial peptides are important for clearance of bacterial infection, and induction of type I IFNs by influenza virus A has been shown to prevent Th17 activation (10-11, 13). Our results suggest that MRSA challenge downregulates pro-inflammatory pathways and genes associated with anti-bacterial clearance, such as IL-17a, IL-23a, LCN2, IL-1α, IL-1β, and S100A8-9 consistent with previous findings (11). During influenza virus infection, pro-inflammatory cytokines IFNγ and TNFα are upregulated, but we found that expression of these cytokines by lung $CD8^+$ T cells decreased significantly due to MRSA infection in WT

mice. IFNγ has been shown previously to impair control of secondary bacterial pneumonias, so downregulation of IFNγ in our model may be beneficial (13, 43-44). However, downregulation of TNFα may be detrimental for bacterial clearance as it has been shown to be protective against *S. aureus* (45-47). Together, these data show that despite memory training of immune cells, secondary challenge with MRSA alters $CD8^+$ T cell phenotype; however, these cells appear to be able to effectively mount an anti-bacterial response against MRSA. Further investigation is needed to uncover phenotypic and functional changes in $CD8^+$ T cells during super-infection.

B cells have been shown to be integral to maintaining tissue integrity, primarily by immunoregulating key effector cells that drive tissue damage; neutrophils and macrophages (48-50). We observed that loss of B cells increased lung injury and inflammation, but this finding was seen only after heterotypic memory, not acute super-infection. Increased inflammation and immune cell recruitment in B cell deficient lungs was particularly concentrated towards the blood vessels, rather than the parenchyma. A similar finding has been seen in lungs of $Rag2^{-/-}$ mice, which lack mature B and T cells (51). We examined if the cause of increased lung tissue injury was due to lack of antibody or due to other antibody-independent B cell functions (48-50). Using MD4 and IgMi mice in addition to μMT mice showed that lung tissue injury during memory super-infection was caused primarily by loss of antibody. IgMi mice have been reported previously to secrete more IL-10, an important immunoregulatory cytokine, but increased B cell derived IL-10 did not rescue lung tissue injury (40, 52). Depleting $CD8^+$ T cells did not rescue lung tissue injury. There was an increase of cytokines in the lungs of B cell deficient mice that are associated with immunopathology, particularly IL-6,

MCP-1, MIP-1β, and G-CSF (53-56). Cytokine increases suggests that absence of B cell immunoregulatory signals to neutrophils and macrophages may cause increased lung tissue inflammation during memory super-infection. Additionally, we saw increased inflammatory macrophages in B cell deficient mice compared to WT mice. While, there was no difference in total neutrophil number between WT and B cell deficient lungs, the neutrophils of B cell deficient mice appeared to be more mature and had increased iNOS expression, which was shown to increase tissue damage (57-59). Influenza memory antibody serum add back to B cell deficient mice at the beginning of super-infection rescued weight loss, lung injury, and decreased numbers of activated $CD8^+$ T cells and macrophages. Overall, these findings show that loss of antibody production by B cells leads to a more inflammatory environment, leading to increased lung injury. However, the immunological mechanisms underlying this increased lung injury require further investigation.

Clinically, depletion of B cells via monoclonal antibodies like Rituximab increases patient risk of higher morbidity and mortality to infectious diseases (60). Previous studies have shown that loss of B cells accelerates the contraction of memory $CD8^+$ T cells formed in response to infection and vaccination (61-66). Rituximab-treated rheumatoid arthritis patients were shown to have impaired expansion of influenza virus-specific $CD8^+$ T cells following influenza vaccination, a finding also seen in B cell deficient mice challenged with influenza virus (62). However, a different study examining responses to COVID-19 mRNA vaccines in Rituximab-treated patients showed that the expansion of antigen-specific $CD8^+$ T cells was not impaired, but rather the $CD8^+$ T cells were more activated and expressed more effector molecules (63). We observed that

545 expansion of effector and resident memory $CD8^+$ T cells in B cell deficient mice was not
546 impaired. The number of lung $CD8^+$ T cells and influenza virus-specific $CD8^+$ T cells was
547 significantly higher in B cell deficient mice compared to WT. Additionally, we saw an
548 increased population of CD8 TRMs in the lungs of B cell deficient mice compared to WT.
549 We did not observe impairment in the formation of memory $CD8^+$ T cells in B cell
550 deficient models during heterotypic memory super-infection. The difference in findings is
551 possibly due to natural infection rather than vaccination for the primary challenge.

552 We observed that $CD8^+$ T cells in B cell deficient mice expressed more T cell
553 regulatory markers (PD-1, LAG-3, TIM-3) than WT $CD8^+$ T cells with expression further
554 increased after MRSA challenge. $CD8^+$ T cells in B cell deficient mice had a diminished
555 anti-viral phenotype, expressing lower levels of IFNγ and TNFα compared to WT $CD8^+$
556 T cells. However, the $CD8^+$ T cells expressed significantly more granzyme B compared
557 to WT, a finding that is consistent with a previous study showing impaired $CD8^+$ T cell
558 responses in MD4 mice (61). We also found genes commonly associated with T cell
559 regulation and exhaustion were increased in $CD8^+$ T cells from B cell deficient mice
560 compared to WT. This suggests that B cell deficiency may be driving $CD8^+$ T cells
561 towards a state of terminal effector differentiation. It is clear that B cells are critically
562 involved in regulating memory $CD8^+$ T cell responses, but it is unclear what
563 mechanism(s) are responsible. We found that loss of antibody secretion by B cells was
564 responsible for the increase in lung effector $CD8^+$ T cells as the $CD8^+$ T cells observed
565 in IgMi mice were very similar to those seen in μMT mice. B cells from IgMi mice have
566 been previously shown to have a higher propensity to secrete IL-10 and participate in
567 germinal center reactions compared to WT mice (40). We saw that IgMi mice had a

higher proportion of effector memory $CD8^+$ T cells compared to µMT mice, which may be due to increased germinal center interactions. Depletion of B cells in MD4 mice and adding back influenza antibody serum showed that loss of antibody results in increased memory $CD8^+$ T cells during secondary challenge. Studies are needed to show mechanistically how loss of antibodies during primary infection impacts $CD8^+$ T cell responses. We theorize that lack of antibody results in prolonged engagement of antigen with T cell receptors on $CD8^+$ T cells, which has been shown to increase the magnitude of cytotoxic T lymphocyte activity in $CD8^+$ T cells (67-69).

Heterotypic influenza memory resulted in lower MRSA burden in the lung during super-infection compared to previously naïve mice (32), so it was interesting that loss of memory B cells did not impact MRSA burden. However, secondary challenge with *Klebsiella pnuemoniae* did result in higher bacterial burdens in IgMi mice compared to WT, which could be due to increased virulence or increased ability to evade host immune responses (70). Cytotoxic $CD8^+$ T cells are important mediators of intracellular pathogen killing through production of cytokines, such as IFNγ, TNFα, and granzyme b, and killing of infected cells (71). While only a subset of the $CD8^+$ T cells (15-50%) in our B cell deficient mice were influenza virus-specific, a majority of them expressed granzyme B. This suggests bystander activation of $CD8^+$ T cells, which produce high levels of granzyme b and perforin (72). Depleting $CD8\beta^+$ T cells prior to super-infection increased viral and MRSA burden only in µMT lungs, demonstrating their necessity for viral and bacterial clearance. Challenging WT and µMT mice with lethal-MRSA infection during super-infection resulted in WT mice succumbing within 24-48 hours of infection, which was likely due to higher MRSA burden in the lung. However, µMT mice largely

591 survived initial bacterial infection but succumbed at later time points, likely due to
592 increased weight loss and lung inflammation. The delayed mortality seen in µMT mice
593 was only observed when the mice were challenged with PR8 prior to lethal MRSA
594 infection, suggesting that PR8 infection activated bystander $CD8^+$ T cells, which
595 promoted clearance of secondary bacterial infection. These data show that the cytotoxic
596 effector memory $CD8^+$ T cells that result from B cell deficiency are protective against
597 secondary bacterial challenge, but their contributions towards immunopathology are still
598 unclear. These data suggest that the increased lung tissue injury and inflammation seen
599 in B cell deficient mice during memory super-infection is likely due to immune activation
600 from bacterial challenge rather than bacterial load. Although our findings are limited to
601 two heterotypic influenza virus strains, we believe the immunological findings regarding
602 regulation of $CD8^+$ T cells by B cells is relevant to other anti-microbial immunity and
603 vaccination contexts. Further studies are needed to resolve how B cells and $CD8^+$ T
604 cells regulate each other, which is crucial for providing effective therapeutic
605 interventions to viral and bacterial infections.

606

607

METHODS

Sex as a biological variable

This study examined predominately male animals to reduce experimental variability. We have done some experiments (as indicated) with female mice and similar findings are reported for both sexes.

Mice

Six- to eight-week-old male wild-type (WT) C57BL/6, MD4 (C57BL/6-Tg(IghelMD4)4Ccg/J), and μMT (B6.129S2-Ighmtm1Cgn/J) mice and were purchased from Jackson Laboratories (Bar Harbor, ME). IgMi mice were a gift from the laboratory of Dr. Timothy Hand at UPMC Children's Hospital of Pittsburgh. Mice were maintained under pathogen-free conditions at UPMC Children's Hospital of Pittsburgh. Studies were performed on sex- and age- matched mice.

Mouse model and sampling collection

On day 0, 6- to 8- week male or female mice were infected with 0.5-1 x 10^5 PFU of mouse-adapted influenza virus A/HKx31 H3N2 (X31) or PBS vehicle. After 54 days, the mice were rechallenged with 10^3 PFUs of a heterotypic strain of mouse-adapted influenza virus A/PR/8/34 H1N1 (PR8) or PBS vehicle. Six days after influenza virus rechallenge (day 60), the mice were challenged with 5 x 10^7 CFUs of USA300 MRSA (stationary phase) suspended in PBS or vehicle and harvested a day later. For homotypic influenza virus challenge models, mice were infected with PR8 at both viral challenge time points. For *Klebsiella pnuemoniae* experiments, mice were challenged with 5x10^3 CFUs of *K.pneumoniae* (ATCC 43816) at day 60 and tissues were harvested

48 hours later (day 62). All infections were given via oropharyngeal instillation. Mice were euthanized via pentobarbital injection followed by cervical dislocation and exsanguination by severing the renal artery.

Bronchoalveolar lavage fluid collection and differential cell staining

Bronchoalveolar lavage fluid (BALF) was collected from mice at tissue harvest and processed according to Supplemental Methods.

Bacterial plating

The upper right lung lobes of mice were collected and homogenized in 1 mL of PBS. Neat and 10-fold dilutions of lung homogenate were dot plated and then incubated at 37°C overnight and CFUs were quantified by bacterial colony counting.

Flow cytometry

Flow cytometry was performed on single cell suspensions obtained from lung tissue according to Supplemental Methods.

Histology and Qupath analysis

Histological processing and analysis of lungs was performed as outlined in Supplemental Methods.

RNA extraction and quantitative PCR

Lung tissue was collected at day of harvest and processed for RNA extraction and q-PCR according to Supplemental Methods.

Hemagglutinin Inhibition Assay (HAI)

HAI assays were conducted on serum samples according to Supplemental Methods.

Lincoplex and Protein assays

Protein levels in BALF were determined using the Pierce BCA protein assay kit (Thermo Fisher Scientific, Waltham, MA). Cytokine production was measured using homogenate of upper right lung (1 mL of PBS) using the Bio-Rad Magpix (Hercules, CA) platform with the Bio-Plex Pro Mouse Cytokine 23-plex assay (Bio-Rad, Hercules, CA). BALF was used to determine granzyme B production using Mouse granzyme B DuoSet ELISA kit (R&D Systems, Minneapolis, MN).

CD8β T cell depletion

CD8β T cell depletion was performed twice, five and two days before PR8 challenge (Day 49 and 52). µMT or WT C57BL/6 mice were injected intravenously via tail vein with 200 µg of *InVivo*MAb anti-mouse CD8β (Lyt 3.2, clone: 53-5.8, BioXcell, Lebanon, NH) or 200 µg of *InVivo*MAb rat IgG1 isotype control, anti-horseradish peroxidase (clone: HPRN, BioXcell, Lebanon, NH). Mice were oropharyngeally administered 200 µg of *InVivo*MAb anti-mouse CD8β (Lyt 3.2, clone: 53-5.8, BioXcell, Lebanon, NH) or 200 µg of *InVivo*MAb rat IgG1 isotype control, anti-horseradish

peroxidase (clone: HPRN, BioXcell, Lebanon, NH). Depletion efficiency was assessed via flow cytometry.

B cell depletion

Early B cell depletion was performed 7 days prior to X-31 (H3N2) challenge. MD4 mice were injected intravenously via tail vein with 250 µg of Ultra-Leaf Purified anti-mouse CD20 Antibody (SA271G2, Biolegend, San Diego, CA) or with 250 µg of Rat IgG2b κ isotype control (RTK4530, Biolegend, San Diego, CA). Mice were oropharyngeally administered 125 µg of Ultra-Leaf Purified anti-mouse CD20 Antibody (SA271G2, Biolegend, San Diego, CA) or with 125 µg of Rat IgG2b κ isotype control (RTK4530, Biolegend, San Diego, CA). Late B cell depletion was performed intravenously and oropharyngeally with identical CD20 antibody and isotype volume and concentrations except treatment was performed 5 days (day 49) and 2 days (day 52) prior to PR8 infection (day 54) in WT (C57BL/6) mice.

Serum transfer experiments

WT or µMT mice were injected intravenously via tail vein with 150µL of PBS vehicle, pooled naïve serum collected from WT mice, or pooled influenza memory serum collected from WT mice with F/F/S infection at day of tissue harvest (day 61). Mice were passively immunized 6-7 hours following PR8 challenge (day 54).

Bulk-RNA sequencing on Lung $CD8^+$ T cells

RNA was extracted from mouse lung $CD8^+$ T cells according to methods outlined in Supplemental Methods. MedGenome (Foster City, CA) performed library preparation (Takara SMART-Seq mRNA, San Jose, CA) and sequencing (Illumina NovaSeq, Oakdale, MN) with 100-bp single-end reads and 20 million reads per sample.

Bioinformatics

Bulk-RNA sequencing reads were aligned and analyzed by MedGenome (Foster City, CA). Gene Set Enrichment Analysis was performed using Webgestalt (WEB-based GEne SeT AnaLysis Toolkit) (73). Heatmaps were made using the provided TPM counts and using R in R Studio version 4.1.0, data were $\log_2$-transformed and scaled according to row using the pheatmap package (74) to highlight expression levels for select genes across samples.

Statistics

Data were analyzed using GraphPad Prism software (San Diego, CA). Experiments were repeated two to six times as indicated. All data are presented as mean with SEM, unless otherwise noted. Mann-Whitney *U* test, one-way ANOVA with multiple comparisons, or two-way ANOVA were used for statistical significance with a *p* value ≤ 0.05.

Study Approval

All research with animal models was subject to prior review and approval and conducted in compliance by University of Pittsburgh's Institutional Animal Care and Use Committee (protocol #23073501).

Data availability

Datasets are available in the NCBI's Gene Expression Omnibus (GEO) repository (GEO GSE288913). Individual data points are graphed to depict experimental variation. Raw data are provided in Supporting Data Values files. Data are available upon request from the corresponding author, subject to institutional review and approval.

ACKNOWLEDGEMENTS

We thank Dr. Timothy Hand and Darryl Abbott for gifting IgMi mice. We thank Brian Campfield and Mattew Henkel for gifting the *Klebsiella pnuemoniae* strain used. We thank Dr. Jishnu Das and Priyamvada Guha Roy for technical assistance on our bulk-RNA-seq analysis. We thank Dr. Keven M. Robinson for critical review of this manuscript. We thank the Unified Flow Cytometry Core at the University of Pittsburgh and the UPMC Children's Hospital of Pittsburgh Flow Cytometry Core. We thank the UPMC Children's Hospital of Pittsburgh Histology Core, which processed, stained, and scanned lung samples.

REFERENCES

1. Matrosovich MN, Matrosovich TY, Gray T, Roberts NA, and Klenk HD. Human and avian influenza viruses target different cell types in cultures of human airway epithelium. *Proceedings of the National Academy of Sciences of the United States of America.* 2004;101(13):4620-4.
2. Atkin-Smith GK, Duan M, Chen W, and Poon IKH. The induction and consequences of Influenza A virus-induced cell death. *Cell death & disease.* 2018;9(10):1002.
3. Robinson KM, Kolls JK, and Alcorn JF. The immunology of influenza virus-associated bacterial pneumonia. *Curr Opin Immunol.* 2015;34(59-67).
4. Cipolla EM, Huckestein BR, and Alcorn JF. Influenza sequelae: from immune modulation to persistent alveolitis. *Clin Sci (Lond).* 2020;134(13):1697-714.
5. Louria DB, Blumenfeld HL, Ellis JT, Kilbourne ED, and Rogers DE. Studies on influenza in the pandemic of 1957-1958. II. Pulmonary complications of influenza. *The Journal of clinical investigation.* 1959;38(1 Part 2):213-65.
6. van de Sandt CE, Bárcena M, Koster AJ, Kasper J, Kirkpatrick CJ, Scott DP, de Vries RD, Herold S, Rimmelzwaan GF, Kuiken T, et al. Human CD8(+) T Cells Damage Noninfected Epithelial Cells during Influenza Virus Infection In Vitro. *American journal of respiratory cell and molecular biology.* 2017;57(5):536-46.
7. Morens DM, Taubenberger JK, and Fauci AS. Predominant role of bacterial pneumonia as a cause of death in pandemic influenza: implications for pandemic influenza preparedness. *J Infect Dis.* 2008;198(7):962-70.

8. Kuiken T, and Taubenberger JK. Pathology of human influenza revisited. *Vaccine.* 2008;26 Suppl 4(Suppl 4):D59-66.

9. Robinson KM, Choi SM, McHugh KJ, Mandalapu S, Enelow RI, Kolls JK, and Alcorn JF. Influenza A exacerbates Staphylococcus aureus pneumonia by attenuating IL-1β production in mice. *Journal of immunology (Baltimore, Md : 1950).* 2013;191(10):5153-9.

10. Nakamura S, Davis KM, and Weiser JN. Synergistic stimulation of type I interferons during influenza virus coinfection promotes Streptococcus pneumoniae colonization in mice. *J Clin Invest.* 2011;121(9):3657-65.

11. Kudva A, Scheller EV, Robinson KM, Crowe CR, Choi SM, Slight SR, Khader SA, Dubin PJ, Enelow RI, Kolls JK, et al. Influenza A inhibits Th17-mediated host defense against bacterial pneumonia in mice. *J Immunol.* 2011;186(3):1666-74.

12. Ghoneim HE, Thomas PG, and McCullers JA. Depletion of alveolar macrophages during influenza infection facilitates bacterial superinfections. *J Immunol.* 2013;191(3):1250-9.

13. Sun K, and Metzger DW. Inhibition of pulmonary antibacterial defense by interferon-gamma during recovery from influenza infection. *Nat Med.* 2008;14(5):558-64.

14. Small CL, Shaler CR, McCormick S, Jeyanathan M, Damjanovic D, Brown EG, Arck P, Jordana M, Kaushic C, Ashkar AA, et al. Influenza infection leads to increased susceptibility to subsequent bacterial superinfection by impairing NK cell responses in the lung. *J Immunol.* 2010;184(4):2048-56.

15. Narayana Moorthy A, Narasaraju T, Rai P, Perumalsamy R, Tan KB, Wang S, Engelward B, and Chow VT. In vivo and in vitro studies on the roles of neutrophil extracellular traps during secondary pneumococcal pneumonia after primary pulmonary influenza infection. *Front Immunol.* 2013;4(56).

16. Rich HE, McCourt CC, Zheng WQ, McHugh KJ, Robinson KM, Wang J, and Alcorn JF. Interferon Lambda Inhibits Bacterial Uptake during Influenza Superinfection. *Infect Immun.* 2019;87(5).

17. Wasserman MG, Graham RJ, and Mansbach JM. Airway Bacterial Colonization, Biofilms and Blooms, and Acute Respiratory Infection. *Pediatric critical care medicine : a journal of the Society of Critical Care Medicine and the World Federation of Pediatric Intensive and Critical Care Societies.* 2022;23(10):e476-e82.

18. Li N, Ren A, Wang X, Fan X, Zhao Y, Gao GF, Cleary P, and Wang B. Influenza viral neuraminidase primes bacterial coinfection through TGF-β-mediated expression of host cell receptors. *Proceedings of the National Academy of Sciences of the United States of America.* 2015;112(1):238-43.

19. Gomez Lorenzo MM, and Fenton MJ. Immunobiology of influenza vaccines. *Chest.* 2013;143(2):502-10.

20. Krammer F. The human antibody response to influenza A virus infection and vaccination. *Nature reviews Immunology.* 2019;19(6):383-97.

21. Doherty PC, Turner SJ, Webby RG, and Thomas PG. Influenza and the challenge for immunology. *Nature immunology.* 2006;7(5):449-55.

22. Pizzolla A, and Wakim LM. Memory T Cell Dynamics in the Lung during Influenza Virus Infection. *Journal of immunology (Baltimore, Md : 1950).* 2019;202(2):374-81.

23. Zens KD, Chen JK, and Farber DL. Vaccine-generated lung tissue-resident memory T cells provide heterosubtypic protection to influenza infection. *JCI insight.* 2016;1(10).

24. Pizzolla A, Nguyen THO, Smith JM, Brooks AG, Kedzieska K, Heath WR, Reading PC, and Wakim LM. Resident memory CD8(+) T cells in the upper respiratory tract prevent pulmonary influenza virus infection. *Science immunology.* 2017;2(12).

25. Shenoy AT, Wasserman GA, Arafa EI, Wooten AK, Smith NMS, Martin IMC, Jones MR, Quinton LJ, and Mizgerd JP. Lung CD4(+) resident memory T cells remodel epithelial responses to accelerate neutrophil recruitment during pneumonia. *Mucosal immunology.* 2020;13(2):334-43.

26. van de Wall S, Badovinac VP, and Harty JT. Influenza-Specific Lung-Resident Memory CD8(+) T Cells. *Cold Spring Harbor perspectives in biology.* 2021;13(2).

27. Lee S, Yeung KKM, and Watts TH. Tissue-resident memory T cells in protective immunity to influenza virus. *Current Opinion in Virology.* 2024;65(101397.

28. Connors TJ, Ravindranath TM, Bickham KL, Gordon CL, Zhang F, Levin B, Baird JS, and Farber DL. Airway CD8(+) T Cells Are Associated with Lung Injury during Infant Viral Respiratory Tract Infection. *American journal of respiratory cell and molecular biology.* 2016;54(6):822-30.

29. Chowdhury D, and Lieberman J. Death by a thousand cuts: granzyme pathways of programmed cell death. *Annual review of immunology.* 2008;26(389-420).

30. Alexandrova Y, Yero A, Olivenstein R, Orlova M, Schurr E, Estaquier J, Costiniuk CT, and Jenabian M-A. Dynamics of pulmonary mucosal cytotoxic CD8 T-cells in people living with HIV under suppressive antiretroviral therapy. *Respiratory Research.* 2024;25(1):240.

31. Price O, Birrell FA, Mifsud EJ, and Sullivan SG. Epidemiology of repeat influenza infection in Queensland, Australia, 2005–2017. *Epidemiology and Infection.* 2022;150(e144).

32. Cipolla EM, Yue M, Nickolich KL, Huckestein BR, Antos D, Chen W, and Alcorn JF. Heterotypic Influenza Infections Mitigate Susceptibility to Secondary Bacterial Infection. *J Immunol.* 2022;209(4):760-71.

33. Rutigliano JA, Morris MY, Yue W, Keating R, Webby RJ, Thomas PG, and Doherty PC. Protective memory responses are modulated by priming events prior to challenge. *Journal of virology.* 2010;84(2):1047-56.

34. Kreijtz JH, Bodewes R, van Amerongen G, Kuiken T, Fouchier RA, Osterhaus AD, and Rimmelzwaan GF. Primary influenza A virus infection induces cross-protective immunity against a lethal infection with a heterosubtypic virus strain in mice. *Vaccine.* 2007;25(4):612-20.

35. Li H, van der Leun AM, Yofe I, Lubling Y, Gelbard-Solodkin D, van Akkooi ACJ, van den Braber M, Rozeman EA, Haanen J, Blank CU, et al. Dysfunctional CD8 T Cells Form a Proliferative, Dynamically Regulated Compartment within Human Melanoma. *Cell.* 2019;176(4):775-89.e18.

852 36. van der Leun AM, Thommen DS, and Schumacher TN. CD8(+) T cell states in
853 human cancer: insights from single-cell analysis. *Nature reviews Cancer.*
854 2020;20(4):218-32.
855 37. Rha M-S, and Shin E-C. Activation or exhaustion of CD8(+) T cells in patients
856 with COVID-19. *Cellular & molecular immunology.* 2021;18(10):2325-33.
857 38. Jenkins E, Whitehead T, Fellermeyer M, Davis SJ, and Sharma S. The current
858 state and future of T-cell exhaustion research. *Oxford open immunology.*
859 2023;4(1):iqad006.
860 39. Mozdzanowska K, Furchner M, Zharikova D, Feng J, and Gerhard W. Roles of
861 CD4(+) T-cell-independent and -dependent antibody responses in the control of
862 influenza virus infection: evidence for noncognate CD4(+) T-cell activities that
863 enhance the therapeutic activity of antiviral antibodies. *Journal of virology.*
864 2005;79(10):5943-51.
865 40. Sahputra R, Yam-Puc JC, Waisman A, Muller W, and Else KJ. Evaluating the
866 IgMi mouse as a novel tool to study B-cell biology. *Eur J Immunol.*
867 2018;48(12):2068-71.
868 41. Shepherd FR, and McLaren JE. T Cell Immunity to Bacterial Pathogens:
869 Mechanisms of Immune Control and Bacterial Evasion. *International journal of*
870 *molecular sciences.* 2020;21(17).
871 42. Bröker BM, Mrochen D, and Péton V. The T Cell Response to Staphylococcus
872 aureus. *Pathogens (Basel, Switzerland).* 2016;5(1).

43. Greenlee-Wacker MC, and Nauseef WM. IFN-γ targets macrophage-mediated immune responses toward Staphylococcus aureus. *Journal of leukocyte biology.* 2017;101(3):751-8.
44. Verma AK, Bauer C, Palani S, Metzger DW, and Sun K. IFN-γ Drives TNF-α Hyperproduction and Lethal Lung Inflammation during Antibiotic Treatment of Postinfluenza Staphylococcus aureus Pneumonia. *The Journal of Immunology.* 2021;207(5):1371-6.
45. Damjanovic D, Divangahi M, Kugathasan K, Small C-L, Zganiacz A, Brown EG, Hogaboam CM, Gauldie J, and Xing Z. Negative Regulation of Lung Inflammation and Immunopathology by TNF-α during Acute Influenza Infection. *The American journal of pathology.* 2011;179(6):2963-76.
46. Varley CD, Deodhar AA, Ehst BD, Bakke A, Blauvelt A, Vega R, Yamashita S, and Winthrop KL. Persistence of Staphylococcus aureus colonization among individuals with immune-mediated inflammatory diseases treated with TNF-α inhibitor therapy. *Rheumatology.* 2013;53(2):332-7.
47. Giai C, Gonzalez C, Ledo C, Garofalo A, Di Genaro MS, Sordelli DO, and Gomez MI. Shedding of tumor necrosis factor receptor 1 induced by protein A decreases tumor necrosis factor alpha availability and inflammation during systemic Staphylococcus aureus infection. *Infection and immunity.* 2013;81(11):4200-7.
48. Suchanek O, and Clatworthy MR. Homeostatic role of B-1 cells in tissue immunity. *Frontiers in immunology.* 2023;14(1106294).
49. Gawish R, Maier B, Obermayer G, Watzenboeck ML, Gorki AD, Quattrone F, Farhat A, Lakovits K, Hladik A, Korosec A, et al. A neutrophil-B-cell axis impacts

tissue damage control in a mouse model of intraabdominal bacterial infection via Cxcr4. *eLife.* 2022;11.

50. Suchanek O, Ferdinand JR, Tuong ZK, Wijeyesinghe S, Chandra A, Clauder A-K, Almeida LN, Clare S, Harcourt K, Ward CJ, et al. Tissue-resident B cells orchestrate macrophage polarisation and function. *Nature Communications.* 2023;14(1):7081.

51. Teijaro JR, Verhoeven D, Page CA, Turner D, and Farber DL. Memory CD4 T Cells Direct Protective Responses to Influenza Virus in the Lungs through Helper-Independent Mechanisms. *Journal of virology.* 2010;84(18):9217-26.

52. Sun Z, Chen A, Fang H, Sun D, Huang M, Cheng E, Luo M, Zhang X, Fang H, and Qian G. B cell-derived IL-10 promotes the resolution of lipopolysaccharide-induced acute lung injury. *Cell death & disease.* 2023;14(7):418.

53. Liu Q, Zhou YH, and Yang ZQ. The cytokine storm of severe influenza and development of immunomodulatory therapy. *Cellular & molecular immunology.* 2016;13(1):3-10.

54. Coates BM, Staricha KL, Koch CM, Cheng Y, Shumaker DK, Budinger GRS, Perlman H, Misharin AV, and Ridge KM. Inflammatory Monocytes Drive Influenza A Virus-Mediated Lung Injury in Juvenile Mice. *Journal of immunology (Baltimore, Md : 1950).* 2018;200(7):2391-404.

55. Hall MW, Geyer SM, Guo CY, Panoskaltsis-Mortari A, Jouvet P, Ferdinands J, Shay DK, Nateri J, Greathouse K, Sullivan R, et al. Innate immune function and mortality in critically ill children with influenza: a multicenter study. *Crit Care Med.* 2013;41(1):224-36.

56. Tanaka T, Narazaki M, and Kishimoto T. IL-6 in inflammation, immunity, and disease. *Cold Spring Harbor perspectives in biology.* 2014;6(10):a016295.

57. Deniset JF, Surewaard BG, Lee WY, and Kubes P. Splenic Ly6G(high) mature and Ly6G(int) immature neutrophils contribute to eradication of S. pneumoniae. *The Journal of experimental medicine.* 2017;214(5):1333-50.

58. Pfirschke C, Engblom C, Gungabeesoon J, Lin Y, Rickelt S, Zilionis R, Messemaker M, Siwicki M, Gerhard GM, Kohl A, et al. Tumor-Promoting Ly-6G(+) SiglecF(high) Cells Are Mature and Long-Lived Neutrophils. *Cell reports.* 2020;32(12):108164.

59. Saini R, and Singh S. Inducible nitric oxide synthase: An asset to neutrophils. *Journal of leukocyte biology.* 2018;105(1):49-61.

60. Varley CD, and Winthrop KL. Long-Term Safety of Rituximab (Risks of Viral and Opportunistic Infections). *Current rheumatology reports.* 2021;23(9):74.

61. Klarquist J, Cross EW, Thompson SB, Willett B, Aldridge DL, Caffrey-Carr AK, Xu Z, Hunter CA, Getahun A, and Kedl RM. B cells promote CD8 T cell primary and memory responses to subunit vaccines. *Cell reports.* 2021;36(8):109591.

62. Graalmann T, Borst K, Manchanda H, Vaas L, Bruhn M, Graalmann L, Koster M, Verboom M, Hallensleben M, Guzmán CA, et al. B cell depletion impairs vaccination-induced CD8(+) T cell responses in a type I interferon-dependent manner. *Annals of the Rheumatic Diseases.* 2021;80(12):1537-44.

63. Madelon N, Lauper K, Breville G, Sabater Royo I, Goldstein R, Andrey DO, Grifoni A, Sette A, Kaiser L, Siegrist CA, et al. Robust T-Cell Responses in Anti-CD20-Treated Patients Following COVID-19 Vaccination: A Prospective Cohort

Study. *Clinical infectious diseases : an official publication of the Infectious Diseases Society of America.* 2022;75(1):e1037-e45.

64. Van Meerhaeghe T, Néel A, Brouard S, and Degauque N. Regulation of CD8 T cell by B-cells: A narrative review. *Frontiers in immunology.* 2023;14(1125605).

65. Shen H, Whitmire JK, Fan X, Shedlock DJ, Kaech SM, and Ahmed R. A Specific Role for B Cells in the Generation of CD8 T Cell Memory by Recombinant Listeria monocytogenes 1. *The Journal of Immunology.* 2003;170(3):1443-51.

66. Asano MS, and Ahmed R. CD8 T cell memory in B cell-deficient mice. *The Journal of experimental medicine.* 1996;183(5):2165-74.

67. Prlic M, Hernandez-Hoyos G, and Bevan MJ. Duration of the initial TCR stimulus controls the magnitude but not functionality of the CD8(+) T cell response. *The Journal of experimental medicine.* 2006;203(9):2135-43.

68. Iezzi G, Karjalainen K, and Lanzavecchia A. The Duration of Antigenic Stimulation Determines the Fate of Naive and Effector T Cells. *Immunity.* 1998;8(1):89-95.

69. Abdelbary M, Hobbs SJ, Gibbs JS, Yewdell JW, and Nolz JC. T cell receptor signaling strength establishes the chemotactic properties of effector CD8(+) T cells that control tissue-residency. *Nature Communications.* 2023;14(1):3928.

70. Sá-Pessoa J, Calderón-González R, Lee A, and Bengoechea JA. Klebsiella pneumoniae emerging anti-immunology paradigms: from stealth to evasion. *Trends in Microbiology.* 2025.

71. Balin SJ, Pellegrini M, Klechevsky E, Won ST, Weiss DI, Choi AW, Hakimian J, Lu J, Ochoa MT, Bloom BR, et al. Human antimicrobial cytotoxic T lymphocytes,

defined by NK receptors and antimicrobial proteins, kill intracellular bacteria. *Science immunology.* 2018;3(26):eaat7668.

72. Kim T-S, and Shin E-C. The activation of bystander CD8(+) T cells and their roles in viral infection. *Experimental & Molecular Medicine.* 2019;51(12):1-9.

73. Zhang B, Kirov S, and Snoddy J. WebGestalt: an integrated system for exploring gene sets in various biological contexts. *Nucleic acids research.* 2005;33(Web Server issue):W741-8.

74. Kolde R. 2019.

FIGURE LEGENDS

FIGURE 1. Loss of B cells increases lung populations of T cells and inflammatory macrophages during memory super-infection**. (A)** Infection scheme for memory super-infected mice. **(B)** Representative H&E lung images (40X) with a heatmap overlay to signify lung areas with inflammation/consolidation. **(C)** Lung nucleated cell density (cells/mm^2) and frequency of lung inflammation and consolidation detections between WT vs. µMT lungs and between F/F and F/F/S treatment groups (WT-F/F: *n*=12, WT-F/F/S: *n*=18, µMT-F/F: *n*=12, µMT-F/F/S: *n*=18). **(D)** Flow cytometry analysis was conducted on WT and µMT mice with F/F and F/F/S infections. Samples were concatenated (*n*=4) and populations were visualized using FlowSOM and tSNE-CUDA using Cytobank software. **(E-F)** Samples were analyzed by flow cytometry. Absolute number of $CD64^+CD11b^+CD11c^{lo}$ cells (WT-F/F: *n*=12, WT-F/F/S: *n*=11, µMT-F/F: *n*=12, µMT-F/F/S: *n*=13) and percentage of $iNOS^+MHCII^{hi}$ cells of $CD64^+$ cells (WT-F/F: *n*=7, WT-F/F/S: *n*=8, µMT-F/F: *n*=7, µMT-F/F/S: *n*=8). Data represented as mean ± SEM and *P* values were determined by repeated 1-way ANOVA measures (**p* < 0.05, ***p* < 0.01, ****p* <0.001, *****p* < 0.0001).

FIGURE 2. Loss of B cells alters $CD8^+$ T cell number and phenotype during memory super-infection. Flow cytometry analysis was conducted on WT and µMT mice with F/F and F/F/S infections. **(A-B)** Percentage (WT-F/F: *n*=8, WT-F/F/S: *n*=20, µMT-F/F: *n*=8, µMT-F/F/S: *n*=24) and absolute number(WT-F/F: *n*=8, WT-F/F/S: *n*=7, µMT-F/F: *n*=8, µMT-F/F/S: *n*=8) of $CD90.2^+CD8^+$ cells. **(C)** Percentage of $CD4^+CD90.2^+$ cells (WT-F/F: *n*=8, WT-F/F/S: *n*=7, µMT-F/F: *n*=8, µMT-F/F/S: *n*=8). **(D)** Absolute number of

$CD8^+CD69^+CD103^{hi}$ cells (WT-F/F: *n*=8, WT-F/F/S: *n*=7, µMT-F/F: *n*=8, µMT-F/F/S: *n*=8). **(E)** Intracellular flow cytometry plot (left) showing the percentage Granzyme B^+CD8^+ T cells using concatenated F/F/S infected WT and µMT samples (WT-F/F/S: *n*=4, µMT-F/F/S: *n*=4) and absolute number of Granzyme B^+CD8^+ T cells (right) (WT-F/F: *n*=8, WT-F/F/S: *n*=7, µMT-F/F: *n*=8, µMT-F/F/S: *n*=8). **(F-H)** Percentage of $IFN\gamma^+CD8^+$ cells (WT-F/F: *n*=12, WT-F/F/S: *n*=11, µMT-F/F: *n*=12, µMT-F/F/S: *n*=11), $TNF\alpha^+CD8^+$ cells and $Tbet^+CD8^+$ cells (WT-F/F: *n*=8, WT-F/F/S: *n*=7, µMT-F/F: *n*=8, µMT-F/F/S: *n*=8). Data represented as mean ± SEM and *P* values were determined by repeated 1-way ANOVA measures (*$p < 0.05$, **$p < 0.01$, ***$p < 0.001$, ****$p < 0.0001$).

FIGURE 3. Loss of B cells alters the transcriptional state of lung $CD8^+$ T cells during memory super-infection. Bulk-RNA-seq was performed on lung $CD8^+$ T cells from WT and µMT mice with either F/F or F/F/S infections (WT F/F: *n*=4, WT F/F/S: *n*=4, µMT F/F: *n*=3, µMT F/F/S: *n*=3). **(A)** Venn diagram shows the number of statistically significant differentially expressed genes shared between WT F/F vs. WT F/F/S group and µMT F/F vs. µMT F/F/S group. **(B)** Top and bottom 10 GO pathways in µMT F/F/S vs. WT F/F/S on genes with false discovery rate *p*-adjusted values < 0.05 (8831 DEGs). **(C)** Clustering heatmap of $\log_2$ transformed TPM values of WT F/F/S and µMT F/F/S mice for $CD8^+$ T cell genes with adjusted *p*-values (right). **(D)** Flow cytometry analysis showing the percentage of $PD\text{-}1^+LAG\text{-}3^+TIM\text{-}3^+CD8^+$ T cells (WT F/F: *n*=11, WT F/F/S: *n*=10, µMT F/F: *n*=11, µMT F/F/S: *n*=12). **(E)** GSEA of a pathway in µMT F/F/S versus WT F/F/S (top) with *p*-value and enrichment score (bottom). Flow cytometry analysis showing the percentage of $Annexin\text{-}V^+7\text{-}AAD^-CD8^+$ T cells (WT-F/F: *n*=8, WT-F/F/S:

n=7, µMT-F/F: *n*=7, µMT-F/F/S: *n*=8). Graphed data represented as mean ± SEM and *P* values were determined by repeated 1-way ANOVA measures (**$p < 0.01$, ***$p < 0.001$, ****$p < 0.0001$).

FIGURE 4. Loss of influenza virus-specific antibody drives cytotoxic memory $CD8^+$ T cell responses in super-infection. **(A)** X-31 influenza virus-specific serum titers measured by HAI assay at day 61 (WT: *n*=19, MD4: *n*=5, µMT: *n*=8, IgMi: *n*=8). **(B)** Percent weight loss was calculated starting from PR8 infection (WT: *n*=18, MD4: *n*=14, µMT: *n*=26, IgMi: *n*=7). **(C)** Viral burden (PR8) assessed via qPCR (WT: *n*=19, MD4: *n*=14, µMT: *n*=16, IgMi: *n*=8). **(D)** Number of MRSA colonies from lung homogenates (WT: *n*=22, MD4: *n*=9, µMT: *n*=18, IgMi: *n*=8). **(E)** Percentage of $CD8^+$ cells (WT: *n*=27, MD4: *n*=11, µMT: *n*=27, IgMi: *n*=8). **(F)** Percentage of $CD44^{hi}CD62^{lo}CD8^+$ cells (WT: *n*=24, MD4: *n*=11, µMT: *n*=16, IgMi: *n*=8). **(G)** Absolute number of NP-tetramer$^+CD44^{hi}CD8^+$ cells (WT: *n*=19, MD4: *n*=11, µMT: *n*=16, IgMi: *n*=8). **(H)** Percentage of PD-1^+LAG-3^+TIM-3^+CD8^+ cells (WT: *n*=24, MD4: *n*=11, µMT: *n*=16, IgMi: *n*=8). **(I)** Percentage of IFNγ$^+CD8^+$ cells (WT: *n*=19, MD4: *n*=7, µMT: *n*=20, IgMi: *n*=7). **(J)** Median fluorescence intensity (MFI) of Granzyme B^+CD8^+ T cells (WT: *n*=14, MD4: *n*=11, µMT: *n*=13, IgMi: *n*=7). **(K-L)** Protein expression of Granzyme B (WT: *n*=8, MD4: *n*=6, µMT: *n*=7, IgMi: *n*=8) and TNFα (WT: *n*=7, MD4: *n*=7, µMT: *n*=8, IgMi: *n*=7) from BALF. Data represented as mean ± SEM and *P* values were determined by repeated 1-way ANOVA measures (*$p < 0.05$, **$p < 0.01$, ***$p < 0.001$, ****$p < 0.0001$).

FIGURE 5. Loss of influenza virus-specific antibody increases lung tissue injury during memory super-infection. Histology scoring and Qupath analysis was performed on lungs from WT, µMT, MD4, and IgMi mice. **(A)** Representative H&E lung images, scanned at 40X (right). A heatmap overlay was used to signify lung areas with inflammation/consolidation (left). **(B)** Representative histology sections with H&E of WT, µMT, MD4, and IgMi lungs. **(C)** Histology scores of perivascular lung tissue sections. **(D-E)** Quantification of lung nucleated cell density (cells/mm^2) and frequency of lung inflammation and consolidation detections (WT: *n*=17, MD4: *n*=11, µMT: *n*=17, IgMi: *n*=8). **(F)** BALF protein at day of harvest (WT: *n*=30, MD4: *n*=10, µMT: *n*=32, IgMi: *n*=7). Data represented as mean ± SEM and *P* values were determined by repeated 1-way ANOVA measures (*$p < 0.05$, **$p < 0.01$, ****$p < 0.0001$).

FIGURE 6. Temporal B cell depletion during primary influenza virus infection leads to increased lung memory CD8$^+$ T cell formation. **(A)** B Cell depletion scheme. B cells repopulated the lung prior to challenge with PR8 followed by MRSA. **(B)** Depletion efficiency in the lung was confirmed via flow cytometry (Day0-ISO: *n*=4, Day0-B cell-depleted: *n*=4, Day30-ISO *n*=4, Day30-B cell-depleted: *n*=3). **(C)** X-31 influenza virus-specific mouse serum titers measured by HAI assay (ISO: *n*=7, B cell-depleted *n*=5). **(D)** Percent of weight loss for each group (ISO: *n*=14, B cell-depleted *n*=12). **(E-F)** Histology scores of parenchymal lung sections and lung nucleated cell density (cells/mm^2) quantified (ISO: *n*=8, B cell-depleted *n*=7). **(G)** MRSA colonies from lung homogenates (ISO: *n*=6, B cell-depleted *n*=5). **(H-J)** Percentage of lung CD8$^+$ cells, CD8$^+$CD69$^+$CD103^{hi} cells, and PD1$^+$CD8$^+$ cells (ISO: *n*=14, B cell-depleted *n*=11). **(K)**

BALF granzyme B protein concentration (ISO: *n*=6, B cell-depleted *n*=5). Data represented as mean ± SEM and *P* values were determined by repeated 2-tailed Mann-Whitney *U*-test (*$p < 0.05$, **$p < 0.01$, ***$p < 0.001$, ****$p < 0.0001$).

FIGURE 7. Passively immunizing µMT mice with heterotypic memory influenza serum rescues weight loss and tissue injury. WT or µMT mice were intravenously injected with 150 µL of either PBS vehicle, pooled naïve WT serum, or pooled WT memory serum following PR8 challenge (day 54). **(A)** Weight loss for each group. **(B)** Flow cytometry was performed to calculate absolute number of lung $CD8^+CD45^+CD90.2^+$ cells. **(C-D)** Percentage of effector memory $CD44^{hi}CD62^{lo}CD8^+$ cells and $PD1^+CD8^+$ cells. **(E)** Absolute number of $CD64^+CD24^-Ly6g^-CD45^+CD19^-TCR\beta^-$ cells. **(F)** Histology scoring of perivascular lung sections. **(G)** BALF granzyme B protein concentration. For all figures, (WT-vehicle: *n*=12, WT-memory Ab: *n*=8, WT-naïve Ab: *n*=8, µMT-vehicle: *n*=10, µMT-memory Ab: *n*=8, µMT-naïve Ab: *n*=8). Data represented as mean ± SEM and *P* values were determined by repeated 1-way ANOVA measures (*$p < 0.05$, **$p < 0.01$, ***$p < 0.001$, ****$p < 0.0001$).

FIGURE 8. $CD8^+$ T cells induced by B cell deficiency promote bacterial control during memory super-infection. **(A)** $CD8^+$ T cell depletion scheme. **(B)** CD8β T cell depletion was confirmed on day of tissue harvest via flow cytometry (µMT-CD8β-depleted: *n*=8, WT-CD8β-depleted: *n*=8, µMT-ISO: *n*=8, WT-ISO *n*=8). **(C)** MRSA burden in lung homogenates (µMT-CD8β-depleted: *n*=8, WT-CD8β-depleted: *n*=8, µMT-ISO: *n*=7, WT-ISO *n*=7). **(D)** Viral protein (PR8) was assessed via qPCR (µMT-CD8β-depleted: *n*=8,

WT-CD8β-depleted: *n*=8, µMT-ISO: *n*=8, WT-ISO *n*=8). **(E)** BALF granzyme B protein concentration (µMT-CD8β-depleted: *n*=8, WT-CD8β-depleted: *n*=8, µMT-ISO: *n*=8, WT-ISO *n*=8). **(F)** WT and µMT mice were challenged with a lethal dose of MRSA ($2x10^8$) during memory super-infection and weighed daily (left). Weight loss at day of MRSA challenge (Day 60) was compared with day of PR8 challenge (middle) and percent of weight loss 48 hours from MRSA challenge (Day 62) was compared to initial MRSA challenge (right)(WT: *n*=22, µMT: *n*=21). **(G)** Survival percentage was calculated daily following lethal MRSA challenge (left). Median day of mortality was calculated for WT and µMT groups (right)(WT: *n*=22, µMT: *n*=21). **(H)** MRSA burden 14 hours post-lethal MRSA challenge in lung homogenate (WT: *n*=14*,* µMT*: n*=13*).* Data represented as mean ± SEM. For **A-E**, *P* values were determined by repeated 1-way ANOVA measures. For **F-H**, *P* values were determined by repeated 2-tailed Mann-Whitney *U*-test (*$p < 0.05$, **$p < 0.01$, ***$p < 0.001$, ****$p < 0.0001$).

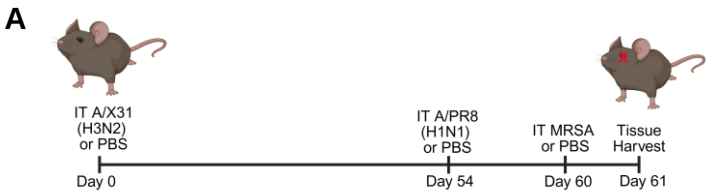

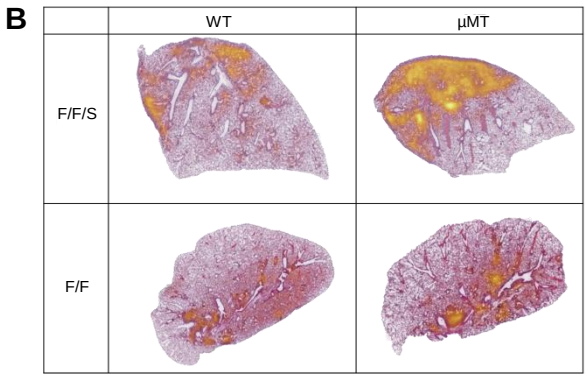

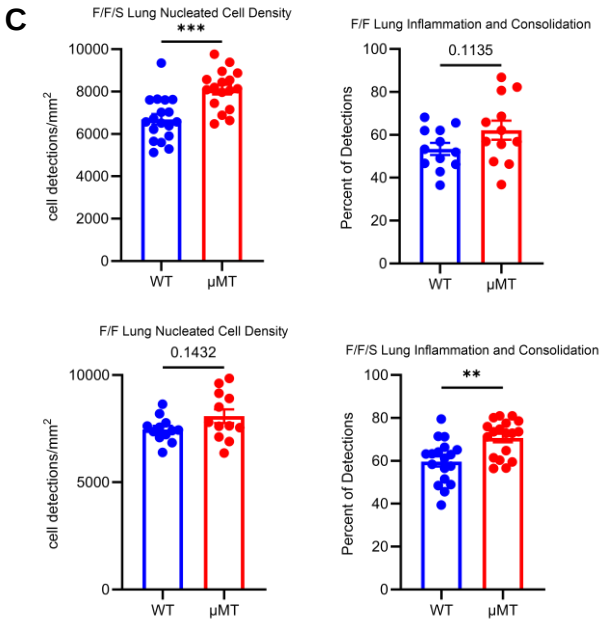

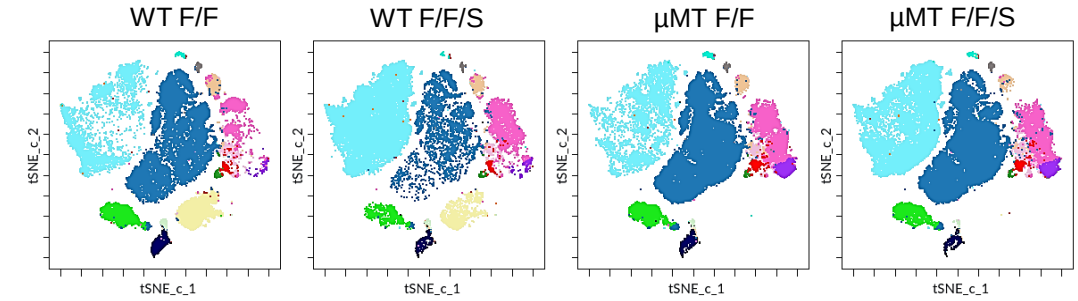

Cluster	Identification	WT FF	WT FFS	μMT FF	μMT FFS
1	Neutrophils	5571	38474	5610	19464
2	Unidentified population	18	68	3	6
3	B cells	11542	1395	0	3
4	Arg1^{lo} Ly6c^{lo} Alveolar Macrophages	120	49	77	37
5	Alveolar Macrophages	120	21	513	234
6	cDC2	1379	540	2216	1305
7	Natural Killer cells	3923	714	2898	1514
8	Interstitial Macrophages	2568	692	655	390
9	NKT cells	1439	389	631	278
10	Inflammatory Ly6c^{hi} Macrophages	3483	3715	6138	4442
11	T cells	18137	3411	28645	21177
12	Unidentified Arg1^{hi} population	320	130	143	90
13	cDC1	475	91	75	54
14	Arg1^{hi} Macrophages	53	92	1760	664
15	Activated DC population	158	182	607	323
16	Eosinophils	694	37	29	19

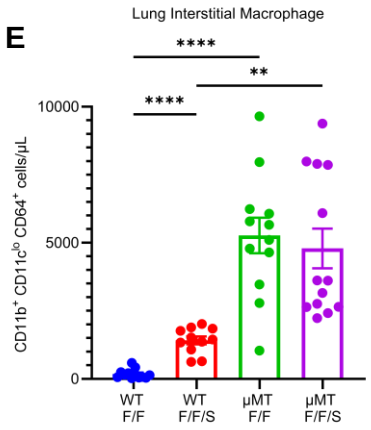

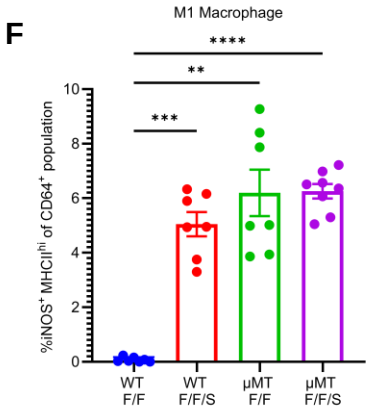

FIGURE 1. Loss of B cells increases lung populations of T cells and inflammatory macrophages during memory super-infection**. (A)** Infection scheme for memory super-infected mice. **(B)** Representative H&E lung images (40X) with a heatmap overlay to signify lung areas with inflammation/consolidation. **(C)** Lung nucleated cell density (cells/mm^2) and frequency of lung inflammation and consolidation detections between WT vs. μMT lungs and between F/F and F/F/S treatment groups (WT-F/F: *n*=12, WT-F/F/S: *n*=18, μMT-F/F: *n*=12, μMT-F/F/S: *n*=18). **(D)** Flow cytometry analysis was conducted on WT and μMT mice with F/F and F/F/S infections. Samples were concatenated (*n*=4) and populations were visualized using FlowSOM and tSNE-CUDA using Cytobank software. **(E-F)** Samples were analyzed by flow cytometry. Absolute number of CD64$^+$CD11b$^+$CD11c^{lo} cells (WT-F/F: *n*=12, WT-F/F/S: *n*=11, μMT-F/F: *n*=12, μMT-F/F/S: *n*=13) and percentage of iNOS$^+$MHCII^{hi} cells of CD64$^+$ cells (WT-F/F: *n*=7, WT-F/F/S: *n*=8, μMT-F/F: *n*=7, μMT-F/F/S: *n*=8). Data represented as mean ± SEM and *P* values were determined by repeated 1-way ANOVA measures (*p < 0.05, **p < 0.01, ***p <0.001, ****p < 0.0001).

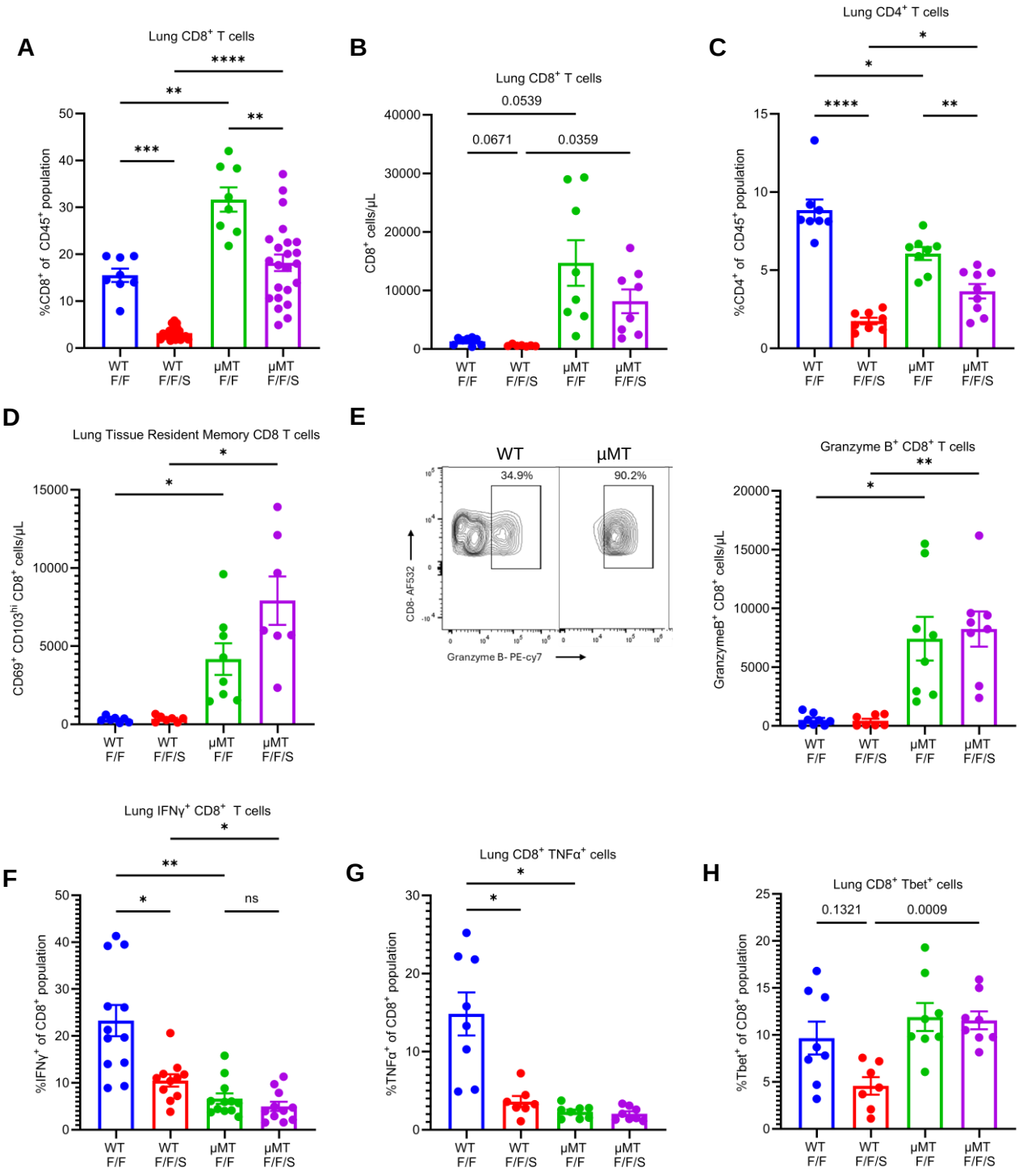

FIGURE 2. Loss of B cells alters CD8⁺ T cell number and phenotype during memory super-infection. Flow cytometry analysis was conducted on WT and µMT mice with F/F and F/F/S infections. **(A-B)** Percentage (WT-F/F: *n*=8, WT-F/F/S: *n*=20, µMT-F/F: *n*=8, µMT-F/F/S: *n*=24) and absolute number(WT-F/F: *n*=8, WT-F/F/S: *n*=7, µMT-F/F: *n*=8, µMT-F/F/S: *n*=8) of CD90.2⁺CD8⁺ cells. **(C)** Percentage of CD4⁺CD90.2⁺ cells (WT-F/F: *n*=8, WT-F/F/S: *n*=7, µMT-F/F: *n*=8, µMT-F/F/S: *n*=8). **(D)** Absolute number of CD8⁺CD69⁺CD103ʰⁱ cells (WT-F/F: *n*=8, WT-F/F/S: *n*=7, µMT-F/F: *n*=8, µMT-F/F/S: *n*=8). **(E)** Intracellular flow cytometry plot (left) showing the percentage Granzyme B⁺CD8⁺ T cells using concatenated F/F/S infected WT and µMT samples (WT-F/F/S: *n*=4, µMT-F/F/S: *n*=4) and absolute number of Granzyme B⁺CD8⁺ T cells (right) (WT-F/F: *n*=8, WT-F/F/S: *n*=7, µMT-F/F: *n*=8, µMT-F/F/S: *n*=8). **(F-H)** Percentage of IFNγ⁺CD8⁺ cells (WT-F/F: *n*=12, WT-F/F/S: *n*=11, µMT-F/F: *n*=12, µMT-F/F/S: *n*=11), TNFα⁺CD8⁺ cells and Tbet⁺CD8⁺ cells (WT-F/F: *n*=8, WT-F/F/S: *n*=7, µMT-F/F: *n*=8, µMT-F/F/S: *n*=8). Data represented as mean ± SEM and *P* values were determined by repeated 1-way ANOVA measures (*$p < 0.05$, **$p < 0.01$, ***$p < 0.001$, ****$p < 0.0001$).

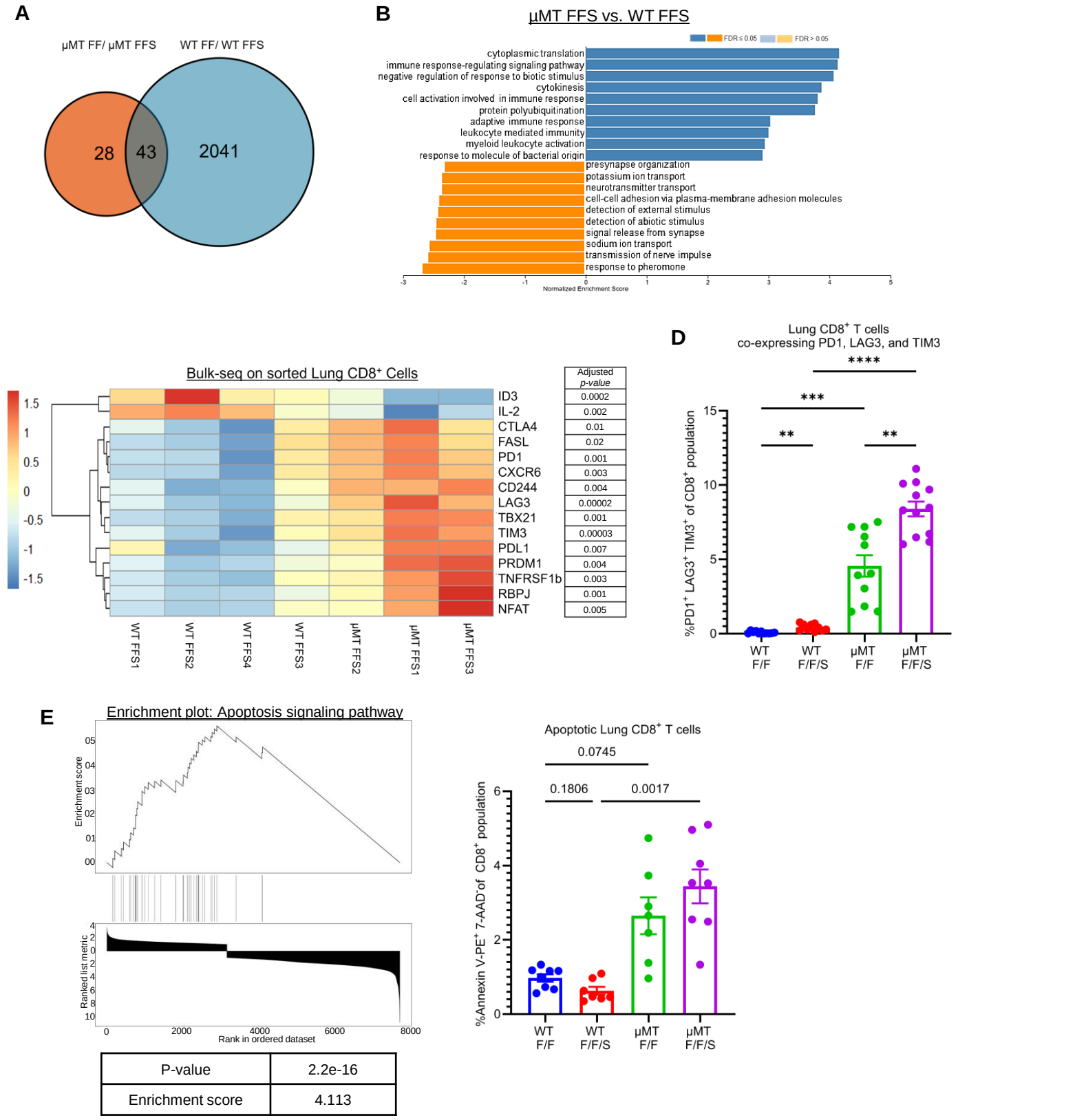

FIGURE 3. Loss of B cells alters the transcriptional state of lung CD8⁺ T cells during memory super-infection. Bulk-RNA-seq was performed on lung CD8⁺ T cells from WT and μMT mice with either F/F or F/F/S infections (WT F/F: *n*=4, WT F/F/S: *n*=4, μMT F/F: *n*=3, μMT F/F/S: *n*=3). **(A)** Venn diagram shows the number of statistically significant differentially expressed genes shared between WT F/F vs. WT F/F/S group and μMT F/F vs. μMT F/F/S group. **(B)** Top and bottom 10 GO pathways in μMT F/F/S vs. WT F/F/S on genes with false discovery rate *p*-adjusted values < 0.05 (8831 DEGs). **(C)** Clustering heatmap of $\log_2$ transformed TPM values of WT F/F/S and μMT F/F/S mice for CD8⁺ T cell genes with adjusted *p*-values (right). **(D)** Flow cytometry analysis showing the percentage of PD-1⁺LAG-3⁺TIM-3⁺CD8⁺ T cells (WT F/F: *n*=11, WT F/F/S: *n*=10, μMT F/F: *n*=11, μMT F/F/S: *n*=12). **(E)** GSEA of a pathway in μMT F/F/S versus WT F/F/S (top) with *p*-value and enrichment score (bottom). Flow cytometry analysis showing the percentage of Annexin-V⁺7-AAD⁻CD8⁺ T cells (WT-F/F: *n*=8, WT-F/F/S: *n*=7, μMT-F/F: *n*=7, μMT-F/F/S: *n*=8). Graphed data represented as mean ± SEM and *P* values were determined by repeated 1-way ANOVA measures (***p* < 0.01, ****p* <0.001, *****p* < 0.0001).

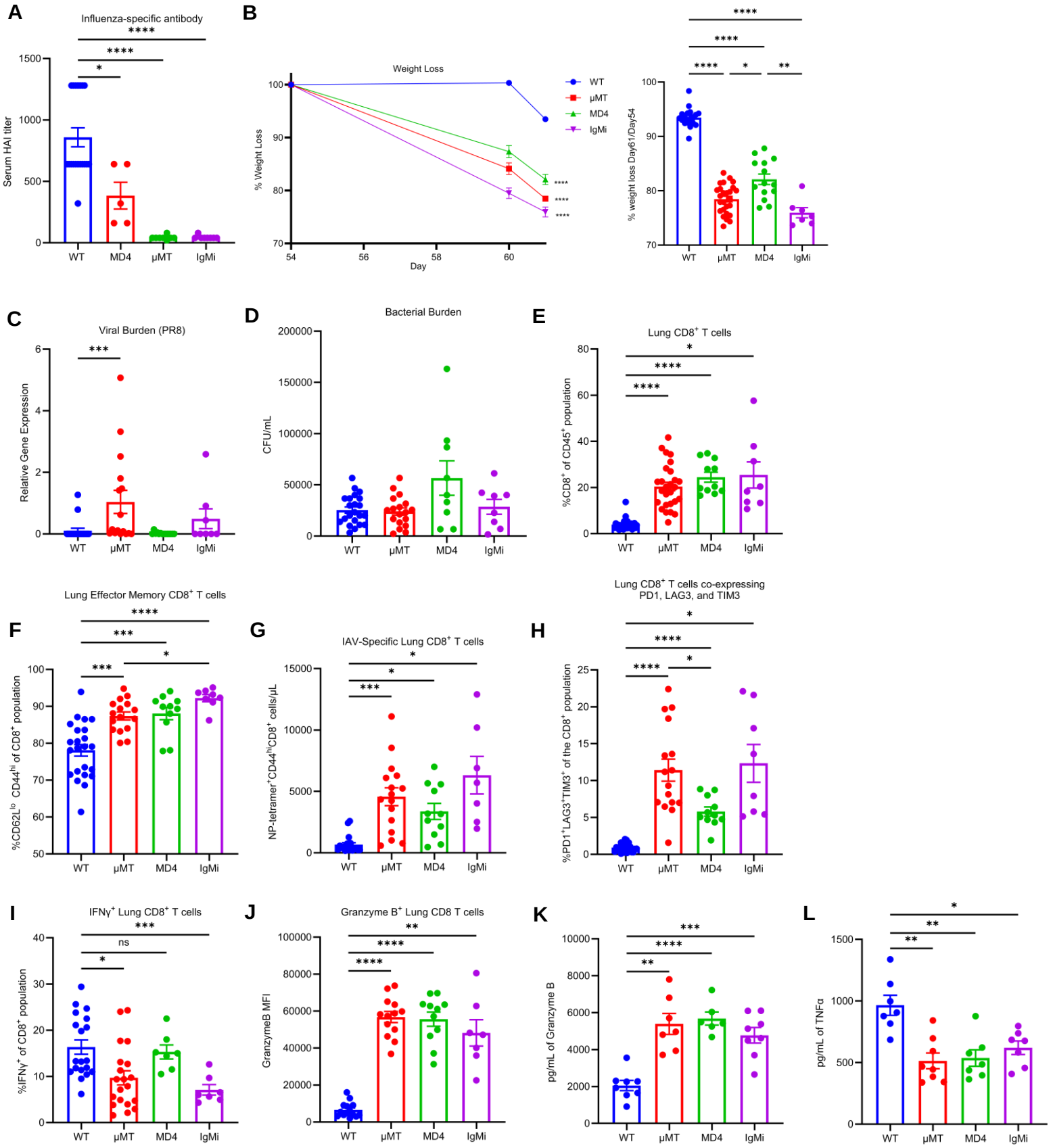

FIGURE 4. Loss of influenza virus-specific antibody drives cytotoxic memory CD8$^+$ T cell responses in super-infection. **(A)** X-31 influenza virus-specific serum titers measured by HAI assay at day 61 (WT: *n*=19, MD4: *n*=5, µMT: *n*=8, IgMi: *n*=8). **(B)** Percent weight loss was calculated starting from PR8 infection (WT: *n*=18, MD4: *n*=14, µMT: *n*=26, IgMi: *n*=7). **(C)** Viral burden (PR8) assessed via qPCR (WT: *n*=19, MD4: *n*=14, µMT: *n*=16, IgMi: *n*=8). **(D)** Number of MRSA colonies from lung homogenates (WT: *n*=22, MD4: *n*=9, µMT: *n*=18, IgMi: *n*=8). **(E)** Percentage of CD8$^+$ cells (WT: *n*=27, MD4: *n*=11, µMT: *n*=27, IgMi: *n*=8). **(F)** Percentage of CD44^{hi}CD62^{lo}CD8$^+$ cells (WT: *n*=24, MD4: *n*=11, µMT: *n*=16, IgMi: *n*=8). **(G)** Absolute number of NP-tetramer$^+$CD44^{hi}CD8$^+$ cells (WT: *n*=19, MD4: *n*=11, µMT: *n*=16, IgMi: *n*=8). **(H)** Percentage of PD-1$^+$LAG-3$^+$TIM-3$^+$CD8$^+$ cells (WT: *n*=24, MD4: *n*=11, µMT: *n*=16, IgMi: *n*=8). **(I)** Percentage of IFNγ$^+$CD8$^+$ cells (WT: *n*=19, MD4: *n*=7, µMT: *n*=20, IgMi: *n*=7). **(J)** Median fluorescence intensity (MFI) of Granzyme B$^+$CD8$^+$ T cells (WT: *n*=14, MD4: *n*=11, µMT: *n*=13, IgMi: *n*=7). **(K-L)** Protein expression of Granzyme B (WT: *n*=8, MD4: *n*=6, µMT: *n*=7, IgMi: *n*=8) and TNFα (WT: *n*=7, MD4: *n*=7, µMT: *n*=8, IgMi: *n*=7) from BALF. Data represented as mean ± SEM and *P* values were determined by repeated 1-way ANOVA measures (*$p < 0.05$, **$p < 0.01$, ***$p < 0.001$, ****$p < 0.0001$).

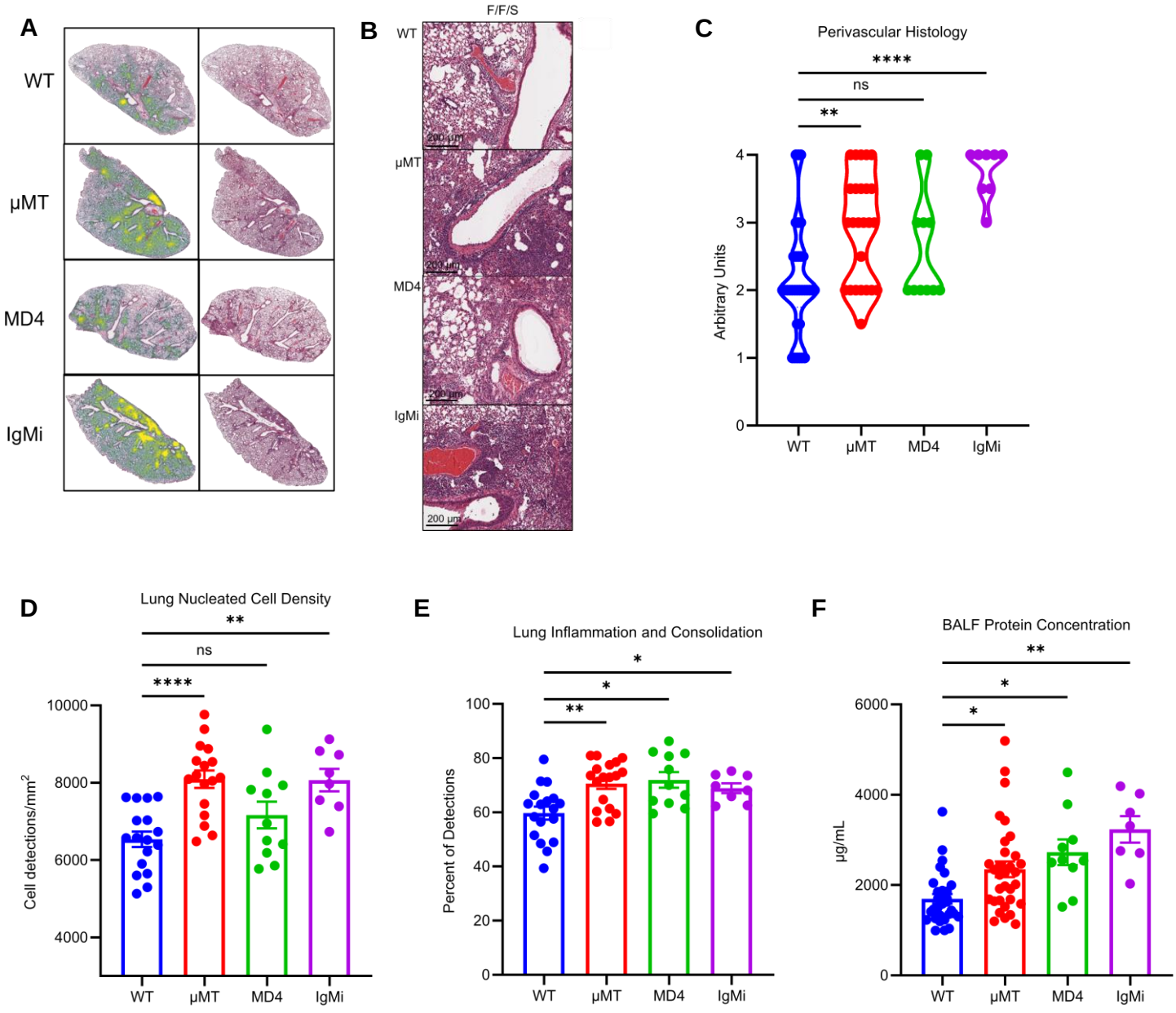

FIGURE 5. Loss of influenza virus-specific antibody increases lung tissue injury during memory super-infection. Histology scoring and Qupath analysis was performed on lungs from WT, µMT, MD4, and IgMi mice. **(A)** Representative H&E lung images, scanned at 40X (right). A heatmap overlay was used to signify lung areas with inflammation/consolidation (left). **(B)** Representative histology sections with H&E of WT, µMT, MD4, and IgMi lungs. **(C)** Histology scores of perivascular lung tissue sections. **(D-E)** Quantification of lung nucleated cell density (cells/mm^2) and frequency of lung inflammation and consolidation detections (WT: *n*=17, MD4: *n*=11, µMT: *n*=17, IgMi: *n*=8). **(F)** BALF protein at day of harvest (WT: *n*=30, MD4: *n*=10, µMT: *n*=32, IgMi: *n*=7). Data represented as mean ± SEM and *P* values were determined by repeated 1-way ANOVA measures (*$p < 0.05$, **$p < 0.01$, ****$p < 0.0001$).

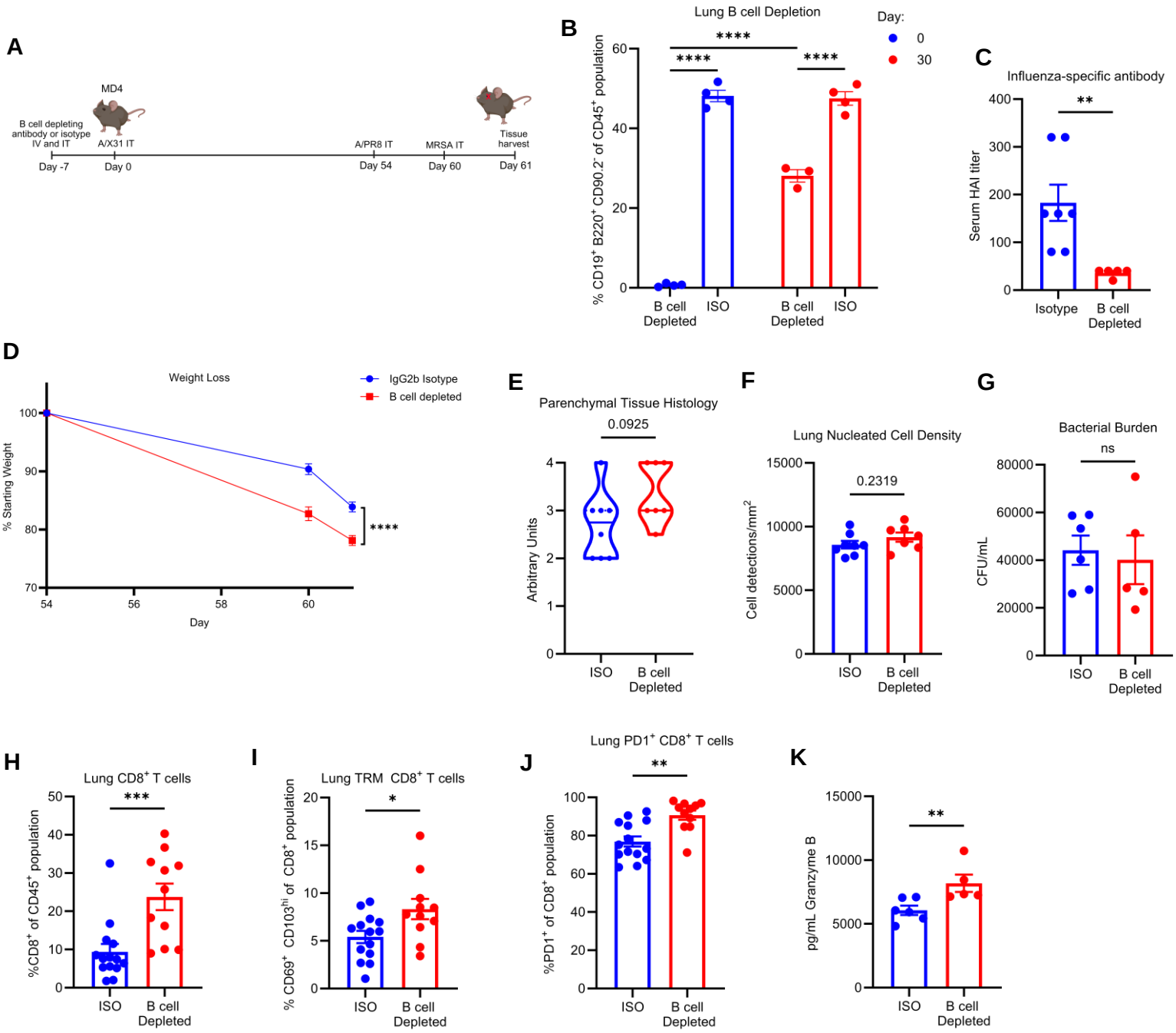

FIGURE 6. Temporal B cell depletion during primary influenza virus infection leads to increased lung memory CD8⁺ T cell formation. **(A)** B cell depletion scheme. B cells repopulated the lung prior to challenge with PR8 followed by MRSA. **(B)** Depletion efficiency in the lung was confirmed via flow cytometry (Day0-ISO: *n*=4, Day0-B cell-depleted: *n*=4, Day30-ISO *n*=4, Day30-B cell-depleted: *n*=3). **(C)** X-31 influenza virus-specific mouse serum titers measured by HAI assay (ISO: *n*=7, B cell-depleted *n*=5). **(D)** Percent of weight loss for each group (ISO: *n*=14, B cell-depleted *n*=12). **(E-F)** Histology scores of parenchymal lung sections and lung nucleated cell density (cells/mm^2) quantified (ISO: *n*=8, B cell-depleted *n*=7). **(G)** MRSA colonies from lung homogenates (ISO: *n*=6, B cell-depleted *n*=5). **(H-J)** Percentage of lung CD8⁺ cells, CD8⁺CD69⁺CD103^{hi} cells, and PD1⁺CD8⁺ cells (ISO: *n*=14, B cell-depleted *n*=11). **(K)** BALF granzyme B protein concentration (ISO: *n*=6, B cell-depleted *n*=5). Data represented as mean ± SEM and *P* values were determined by repeated 2-tailed Mann-Whitney *U*-test (*$p < 0.05$, **$p < 0.01$, ***$p < 0.001$, ****$p < 0.0001$).

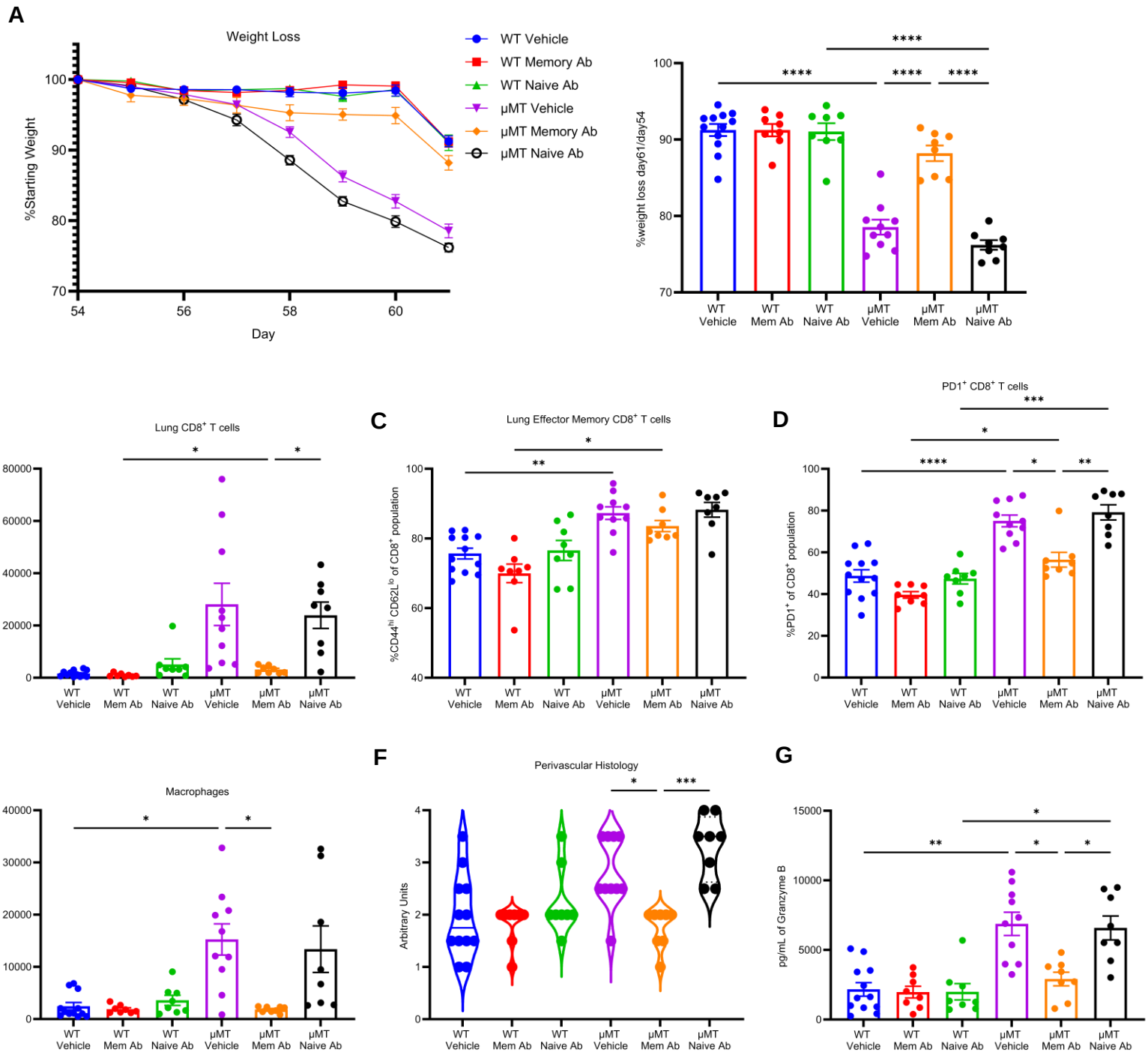

FIGURE 7. Passively immunizing µMT mice with heterotypic memory influenza serum rescues weight loss and tissue injury. WT or µMT mice were intravenously injected with 150 µL of either PBS vehicle, pooled naïve WT serum, or pooled WT memory serum following PR8 challenge (day 54). **(A)** Weight loss for each group. **(B)** Flow cytometry was performed to calculate absolute number of lung $CD8^+CD45^+CD90.2^+$ cells. **(C-D)** Percentage of effector memory $CD44^{hi}CD62^{lo}CD8^+$ cells and $PD1^+CD8^+$ cells. **(E)** Absolute number of $CD64^+CD24^-Ly6g^-CD45^+CD19^-TCR\beta^-$ cells. **(F)** Histology scoring of perivascular lung sections. **(G)** BALF granzyme B protein concentration. For all figures, (WT-vehicle: *n*=12, WT-memory Ab: *n*=8, WT-naïve Ab: *n*=8, µMT-vehicle: *n*=10, µMT-memory Ab: *n*=8, µMT-naïve Ab: *n*=8). Data represented as mean ± SEM and *P* values were determined by repeated 1-way ANOVA measures (*$p < 0.05$, **$p < 0.01$, ***$p < 0.001$, ****$p < 0.0001$).

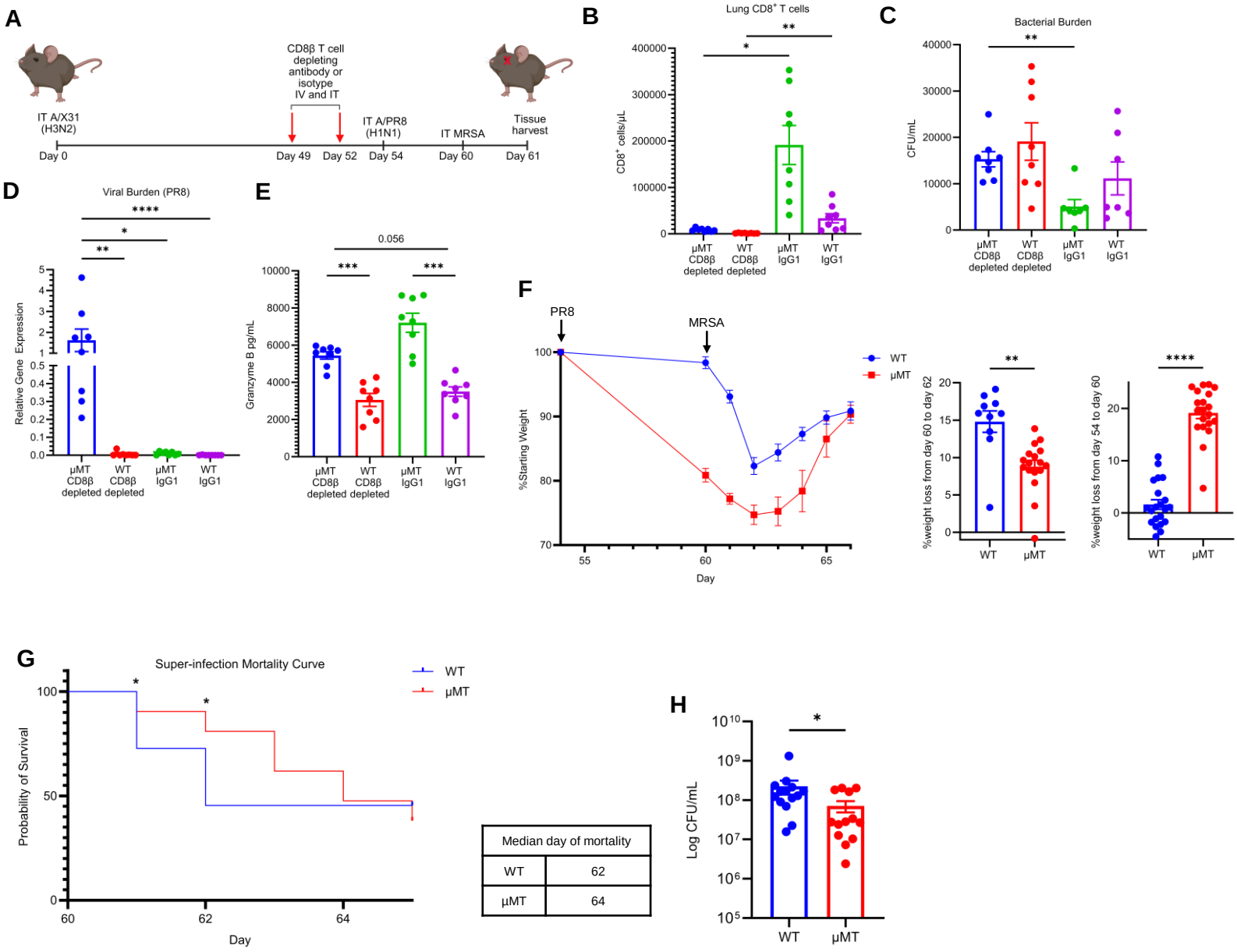

FIGURE 8. CD8⁺ T cells induced by B cell deficiency promote bacterial control during memory super-infection. **(A)** CD8⁺ T cell depletion scheme. **(B)** CD8β T cell depletion was confirmed on day of tissue harvest via flow cytometry (μMT-CD8β-depleted: *n*=8, WT-CD8β-depleted: *n*=8, μMT-ISO: *n*=8, WT-ISO *n*=8). **(C)** MRSA burden in lung homogenates (μMT-CD8β-depleted: *n*=8, WT-CD8β-depleted: *n*=8, μMT-ISO: *n*=7, WT-ISO *n*=7). **(D)** Viral protein (PR8) was assessed via qPCR (μMT-CD8β-depleted: *n*=8, WT-CD8β-depleted: *n*=8, μMT-ISO: *n*=8, WT-ISO *n*=8). **(E)** BALF granzyme B protein concentration (μMT-CD8β-depleted: *n*=8, WT-CD8β-depleted: *n*=8, μMT-ISO: *n*=8, WT-ISO *n*=8). **(F)** WT and μMT mice were challenged with a lethal dose of MRSA ($2x10^8$) during memory super-infection and weighed daily (left). Weight loss at day of MRSA challenge (Day 60) was compared with day of PR8 challenge (middle) and percent of weight loss 48 hours from MRSA challenge (Day 62) was compared to initial MRSA challenge (right)(WT: *n*=22, μMT: *n*=21). **(G)** Survival percentage was calculated daily following lethal MRSA challenge (left). Median day of mortality was calculated for WT and μMT groups (right)(WT: *n*=22, μMT: *n*=21). **(H)** MRSA burden 14 hours post-lethal MRSA challenge in lung homogenate (WT: *n*=14, μMT*: n*=13*)*. Data represented as mean ± SEM. For **A-E**, *P* values were determined by repeated 1-way ANOVA measures. For **F-H**, *P* values were determined by repeated 2-tailed Mann-Whitney *U*-test (*$p < 0.05$, **$p < 0.01$, ***$p < 0.001$, ****$p < 0.0001$).